Deep-Sea Research, Vol. 25, pp. 1121 to 1161
Pergamon Press Ltd. 1978. Printed in Great Britain

0011-7471/78/1201-1121/$02.00/0

The chemistry, biology and vertical flux of particulate matter from the upper 400 m of the Cape Basin in the southeast Atlantic Ocean

JAMES K. B. BISHOP,*† DARLENE R. KETTEN* and JOHN M. EDMOND*

(*Received* 28 *July* 1977; *in revised form* 30 *January* 1978; *final revision received* 11 *May* 1978; *accepted* 15 *May* 1978)

Abstract—Particulate matter, divided into < 1-, 1- to 53- and > 53-μm size fractions, was obtained using the Large Volume *in situ* Filtration System (LVFS), Southlant Expedition, R.V. *Chain* 115, and was analysed for chemical (dry weight, Na, K, Mg, Ca, carbonate, opal, Sr, C, and N), organismal (species assemblage and population densities), and morphological distributions. Profiles from LVFS Stas. 4 to 8 covering regions of low to high productivity and coastal upwelling in the southeast Atlantic are compared with that from LVFS Sta. 2, equatorial Atlantic.

Maxima in organism abundances and particulate mass were generally coincident and occurred at the base of the mixed layer or near-surface when the mixed layer was poorly developed or absent. A consistent distributional pattern of organisms was observed.

Features of the particulate matter distributions attributed to the feeding activities of zooplankton are: strong vertical concentration gradients of mass, organic matter, and organisms; 10-fold enrichment with depth of the > 53-μm fraction with coccolith carbonate; decrease in organic content from 100% at the surface to 50 to 60% at 400 m; fragmentation of most test material below 100 m; and the production of fecal pellets and fecal matter. Coccolithophorids and diatoms were the dominant sources of particulate carbonate and opal.

One- to 53-μm organic C/N ratios were 7.3 ± 0.5 (σ) in productive waters; the < 1-μm ratios were lower. Particulate organic carbon was distributed uniformly below 200 m with concentrations reflecting surface productivity. The calcium to carbonate ratios exceeded unity with values as high as 2.5 being typical of surface waters near Capetown where diatoms dominated; the cycling of excess calcium is 1 to 2×10^{13} mol yr^{-1} or approximately 20% of the annual carbonate precipitation by organisms.

Vertical mass fluxes through 400 m of Foraminifera, fecal pellets, and fecal matter were calculated for three stations using settling models and particle size distributions. Corresponding chemical fluxes of organic carbon, carbonate, and opal are given. Comparisons are made with recalculated fluxes for LVFS Sta. 2.

Over 90% of the organic matter produced in the euphotic zone is recycled in the upper 400 m. The recycling efficiency is nearly 99% in areas of low productivity; the organic to carbonate carbon and the silicate to carbonate ratios are highest at locations where the mass flux is greatest.

INTRODUCTION

THE CHEMISTRY and biology of the vertical flux of particulate matter is of prime importance in determining the removal and regeneration sites of the many elements involved in biogeochemical cycles. Elements such as organic carbon, nitrogen, and phosphorus are fixed by plankton within the surface ocean and are regenerated predominantly in the shallow thermocline. Other biogenic components, such as carbonate and opal, have deeper

* Department of Earth and Planetary Sciences, Massachusetts Institute of Technology, Cambridge, MA 02139, U.S.A.

† Present address: Lamont-Doherty Geological Observatory, Palisades, NY 10964, U.S.A.

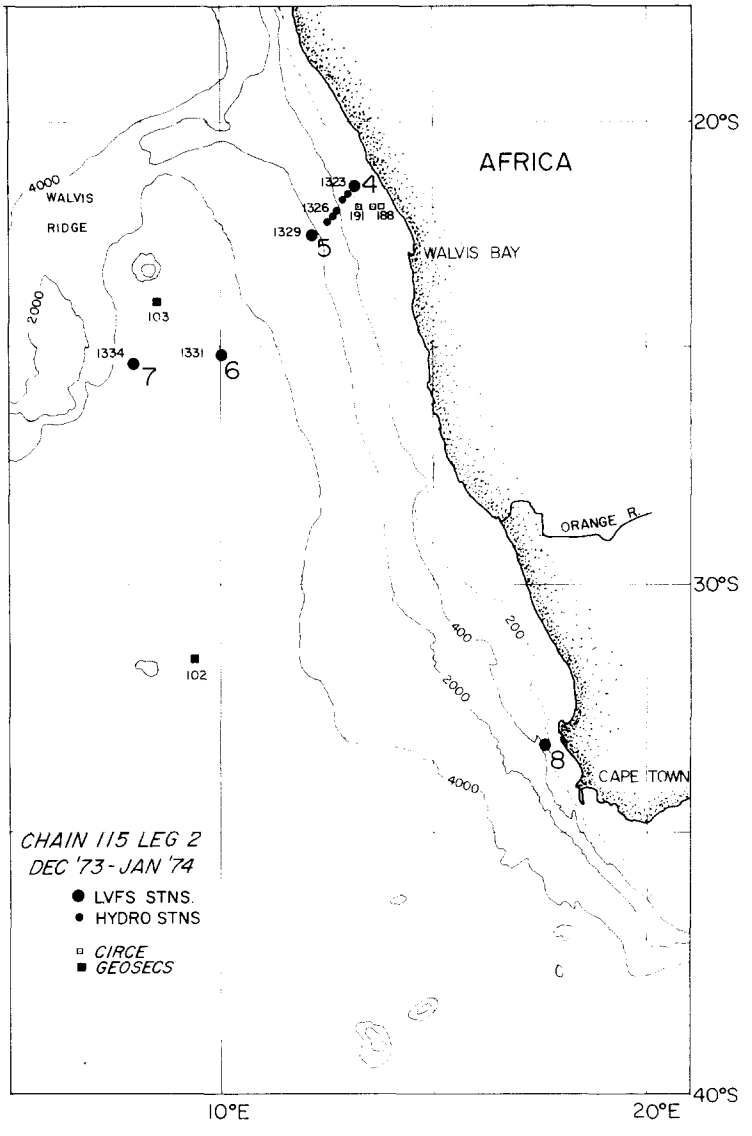

Fig. 1. Station locations for LVFS and hydrographic profiles taken within the Cape Basin. Winds during the survey were less than 10 knots (1 knot = 0.51 m s^{-1}) from the south at Stas. 4 and 5, 15 knots from the south-southeast at Sta. 6, 15 knots from the south at Sta. 8 and increased from 20 to 40 knots from the south-southeast at Sta. 7.

regenerative cycles governed by both the chemistry and physical circulation of the deep ocean. Many other elements are involved in the biogeochemical cycle either actively, as micro-nutrients and skeletal materials, or passively, by adsorption onto particle surfaces or by coprecipitation in carbonate, opal, or celestite phases. Their regeneration is therefore determined by the chemistry and settling behavior of their carriers.

One important feature of deep-sea sediments is the abundance of fine material; e.g. coccoliths, diatom frustules, and detrital clay minerals. Many recent studies suggest that these particles are rapidly sedimented within fecal material (HONJO, 1976; BISHOP, EDMOND,

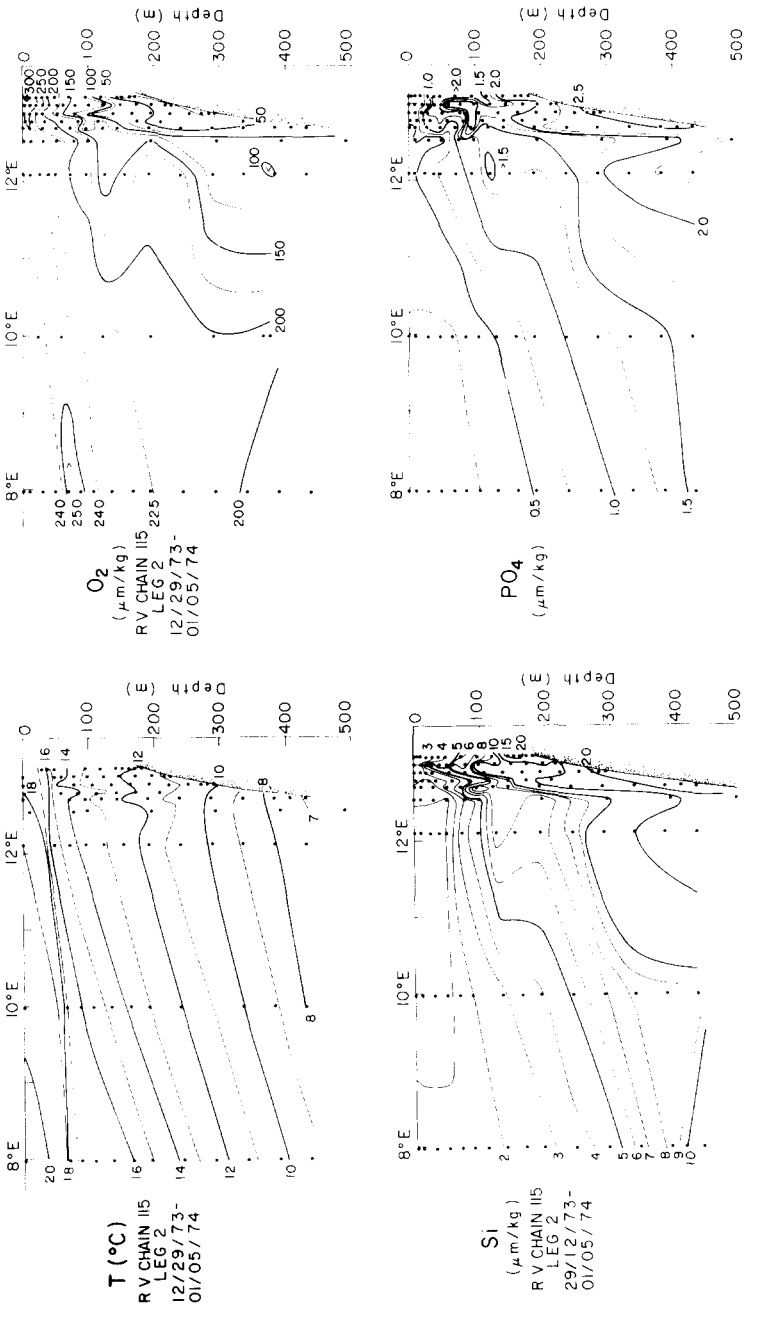

Fig. 2. Temperature, reactive Si, O_2, and PO_4 sections for the stations near Walvis Bay. LVFS Stas. 4 to 7 are nearest the shore, 12, 10, and 8 E. These sections show regeneration of Si and PO_4, and depletion of O_2 in the bottom waters on the shelf.

Table 1. *Particulate matter concentrations; all elemental concentrations reported in* nmol kg^{-1}, z — *sample depth* (m).

LVFS STATION C115 4 21° 28' S 13° 07' E DEC. 28 1973

> 53 MICRON SIZE FRACTION

z	CA	CI	SR	SR*	XS CA	MG	K	NA		WT(I)	DRY WT	SI	SI/CI	CA/CI	SR*/SR
20	45.25		0.195			1.12		100.85	C						
20	55.96	46.10			9.86	4.59		85.00	A	7.31	66.5	37.61	0.816	1.214	0.869
	57.80		0.596	0.518		1.84	2.29	51.88	C						
42	11.75	11.04			0.71	1.51	0.45	2.44	A	2.14	19.4	14.15	1.282	1.065	0.928
	12.66		0.261	0.243		0.63	0.73	12.96	C						
100	7.40	6.36			1.04	0.61	0.12	9.44	A	1.95	4.6	18.48	2.907	1.164	0.915
	8.31		0.128	0.117		0.24	0.03	18.87	C						
183	91.89	83.95			7.95	6.26	0.60	51.85	A	13.41	46.3	70.89	0.845	1.095	0.570
	88.68	83.95			4.74	5.71	1.16	35.03	A					1.056	
	96.79		0.332	0.189		5.63	0.79	23.92	C						

< 53 MICRON SIZE FRACTIONS

	1-53 MICRON SIZE FRACTION						1-53 MICRON FRACTION			<1 MICRON FRACTION								
z	CA	CI	SR	SR*	XS CA	MG	C_{ORG}	N	C_{ORG}/N	C	N	C/N	CHEM WT	DRY WT	SI(CALC)	SI/CI	CA/CI	SR*/SR	TONS
20	536.3	466.5	1.913	1.120	69.8	67.8	17336.	2305.3	7.52	5314.	799.7	6.65	757.17	657.0			1.150	0.585	0.36
							16313.	2253.5	7.24	5221.	717.9	7.27							
20	457.3	372.9	4.188	3.554	84.4	64.2	15944.	2362.8	6.75	2683.	425.7	6.30	632.60	630.2	-34.3	-0.09	1.226	0.849	0.44
							15371.	2325.2	6.61	2721.	429.0	6.34							
							15601.	2315.4	6.74	2702.	501.1	5.39							
42	113.0	105.3	1.035	0.856	7.8	4.0	868.	120.6	7.20	139.	25.1	5.54	43.41	36.1	-104.5	-0.99	1.074	0.827	4.63
100	51.0	44.5	0.458	0.382	6.5	6.5	690.	89.4	7.71	108.	19.2	5.64	30.42	34.3	55.4	1.24	1.146	0.835	6.73
183	253.7	228.5	0.751	0.362	25.2	15.9	1208.	145.2	8.32	111.	21.8	5.08	66.02	90.3	346.9	1.52	1.114	0.483	3.80
	255.4		0.661	0.272	26.9	15.5	1203.	162.3	7.41	89.	20.9	4.25							

TABLE 1 (cont.)

LVFS STATION C115 5 22° 36' S 12° 07' E DEC. 30-31 1973

> 53 MICRON SIZE FRACTION

z	CA	CI	SR	SR*	XS CA	MG	K	NA	
20	129.69	114.72			14.97	13.77	2.77	30.37	A
	140.63		8.541	0.346		10.38	3.46	25.17	C
40	111.54	91.20			20.34	12.05	5.04	39.59	A
	114.87	95.68			19.19	13.85	5.09	52.05	A
	147.14		9.252	9.093		13.72	5.30	34.39	C
50	39.58	35.99			3.59	4.05	0.82	15.02	A
	38.02		0.659	0.598		4.21	0.62	9.20	C
88	63.85	58.33			5.53	3.17	3.83	16.05	A
	74.07	68.08			5.99	3.21	1.51	15.87	A
	65.68		0.514	0.407		4.12	1.01	8.83	C
124	25.82	24.44			1.38	1.48	0.53	6.15	A
	29.22		0.353	0.312		1.81	0.39	2.62	C
199	23.99	22.34			1.65	1.73	0.09	5.34	A
	23.75		0.206	0.168		1.76	0.22	3.19	C
294	11.84	10.51			1.33	0.49	0.45	7.48	A
	11.10		0.103	0.085		0.50	0.37	5.30	C
379	13.83	12.81			1.03	0.29	-0.02	13.03	A
	11.37	10.91			0.45	0.63	0.26	16.41	A
	19.49		0.139	0.119		0.75	0.17	8.60	C
	11.37		0.079	0.058		0.47	0.08	3.45	C

WT(I)	DRY WT	SI	SI/CI	CA/CI	SR*/SR
26.91	103.8	198.78	1.728	1.130	0.977
25.49	88.3	209.66	2.299	1.223	0.983
27.91		237.86	2.486	1.201	
8.25	29.2	64.81	1.801	1.100	0.907
9.08	22.3	45.05	0.772	1.095	0.791
10.05	22.3		0.662	1.088	
4.13	11.8	23.16	0.948	1.056	0.882
3.70	12.3	20.49	0.917	1.074	0.816
2.01	6.3	13.44	1.279	1.126	0.827
2.34	6.1	14.80	1.156	1.080	0.855
1.97	6.1	12.26	1.123	1.041	0.743

1-53 MICRON SIZE FRACTION

z	CA	CI	SR	SR*	XS CA	MG
20	125.7	101.9	1.077	0.903	23.8	43.7
40	68.4	61.0	1.268	1.164	7.4	3.7
50	63.2	55.1	0.966	0.872	8.1	8.3
	64.0		1.017	0.923	8.9	8.2
88	132.2	130.0	0.845	0.627	3.5	4.1
		127.3				
124	139.4	129.9	0.860	0.639	9.4	5.5
199	84.2	79.3	0.583	0.449	4.9	3.1
294	59.1	56.5	0.333	0.237	2.6	0.4
379	79.7	77.5	0.353	0.221	2.2	1.7

1-53 MICRON FRACTION

C_{ORG}	N	C_{ORG}/N
2605.	364.1	7.15
2511.	361.9	6.94
1085.	145.5	7.45
744.	108.3	6.87
465.	64.0	7.26
468.	64.3	7.27
321.	42.8	7.50
368.	41.8	8.81
374.	49.1	7.62
323.	41.2	7.84
295.	37.8	7.82
204.	27.8	7.34
197.	28.9	6.83
197.	26.3	7.50
212.	29.0	7.30
224.	32.7	6.86

<53 MICRON SIZE FRACTIONS

<1 MICRON FRACTION

C	N	C/N
759.	108.7	6.99
555.	231.2	2.40
477.	75.7	6.30
176.	24.3	7.24
61.	9.4	6.44
54.	9.8	5.48
103.	10.3	10.06
41.	5.6	7.20
47.	7.0	6.72
43.	6.9	6.30
48.	7.4	6.46
43.	6.9	6.22
49.	7.8	6.32
47.	9.0	5.23
68.	9.3	7.39
43.	8.5	5.02

CHEM WT	DRY WT	SI(CALC)	SI/CI	CA/CI	SR*/SR	TONS
116.39	132.5	230.2	2.26	1.234	0.839	1.59
56.69	77.8	301.6	4.95	1.121	0.918	2.34
35.71	44.1	119.8	2.17	1.154	0.903	4.49
30.00	33.7	52.9	0.41	1.028	0.741	7.29
26.92	32.7	82.5	0.64	1.073	0.743	8.63
19.59	24.3	67.3	0.85	1.062	0.769	11.74
13.71	14.8	15.6	0.28	1.046	0.712	15.42
16.88	20.4	50.4	0.65	1.028	0.627	13.25

TABLE 1 (cont.)

LWFS STATION C115 6 25° 10' S 10° 01' E JAN. 3 1974

> 53 MICRON SIZE FRACTION

Z	CA	CI	SR	SR*	XS CA	MG	K	NA		WT(I)	DRY WT	SI	SI/CI	CA/CI	SR*/SR
26	14.02	10.23			3.79	4.07	1.33	32.69	A	4.43	18.5	43.27	4.229	1.370	0.991
	14.28	11.88			2.40	-0.29	1.01	64.11	A	4.60	18.5		3.642	1.202	
	18.47		2.064	2.045		3.21	3.21	69.27	C						
52	71.18	54.80			16.38	9.80	2.40	29.71	A	38.60	93.1	466.67	8.516	1.299	0.964
	68.66	53.17			15.49	8.78	2.40	38.90	A	37.36	93.1	451.22	8.486	1.291	
	70.28		2.516	2.425		10.04	4.39	52.16	C						
113	13.60	11.67			1.93	0.89	0.23	12.17	A	3.67	9.1	35.10	3.009	1.166	0.921
	15.52		0.250	0.230		0.98	0.36	7.03	C						
187	10.23	9.91			0.32	0.26	0.04	9.42	A	2.12	5.3	15.78	1.593	1.032	0.878
	11.73		0.139	0.121		0.31	0.65	5.53	C						
289	10.99	10.98			0.01	0.13	0.04	10.56	A	2.13	3.8	14.57	1.326	1.001	0.802
	11.73		0.094	0.076		0.26	0.15	8.76	C						
386	9.65	9.51			0.13	0.33	0.04	1.48	A	1.66	3.1	9.97	1.048	1.014	0.758
	9.22		0.067	0.051		0.22	0.10	6.50	C						0.794
	9.29		0.079	0.063		0.23	0.10	4.33	C						

< 53 MICRON SIZE FRACTIONS

	1-53 MICRON SIZE FRACTION						1-53 MICRON FRACTION			<1 MICRON FRACTION							
Z	CA	CI	SR	SR*	XS CA	MG	C_{ORG}	N	C_{ORG}/N	C	N	C/N	CHEM WT	DRY WT	SI(CALC)	SI/CI	CA/CI	SR*/SR	TONS
26	17.2	14.1			3.1	-8.8	441.	57.4	7.68	207.	35.3	5.87	25.45				1.219		3.46
		14.2					585.	83.2	7.04	214.	33.4	6.41							
							530.	61.9	8.56	289.	41.9	6.89							
26 W	22.3	16.9	0.231	0.202	5.4	-1.0	414.	52.4	7.90	130.	15.1	8.63	18.98	22.9	56.0	3.31	1.319	0.875	3.46
							407.	50.8	8.01	123.	16.7	7.34							
52 W	27.3	26.0	0.186	0.141	1.3	-9.7	604.	104.2	5.79	152.	28.4	5.35	27.03	14.5	-179.1	-6.89	1.088	0.762	2.46
	29.2		0.139	0.095	3.3	-9.4													
113	38.5	35.1	0.352	0.293	3.4	1.2	256.	36.7	6.97	63.	10.7	5.91	13.99	17.1	44.4	1.26	1.096	0.830	9.72
187	67.4	63.4	0.422	0.314	4.0	1.5	157.	21.8	7.20	26.	3.4	7.42	12.44	13.9	20.8	0.33	1.063	0.744	15.97
289	67.3	62.8	0.346	0.240	4.6	1.6	130.	17.4	7.47	18.	2.7	6.88	11.23	13.5	32.5	0.52	1.073	0.692	20.76
							125.	17.1	7.35	19.	2.5	7.77							
386	65.8	63.5	0.318	0.210	2.3	1.8	130.	18.7	6.99	13.	2.0	6.40	11.12	12.6	21.2	0.33	1.036	0.660	22.62

W. SAMPLE REWASHED IN THE LAB AFTER DRYING BEFORE ANALYSIS
MATERIAL LOSS IS INDICATED

TABLE 1 (cont.)

LVFS STATION C115 7 25° 22' S 7° 58' E JAN. 5 1974

Z	CA	CI	SR	SR*	XS CA	MG	K	NA	
20	4.21	3.85			0.36	0.04	0.08	62.87	A
	3.72		0.243	0.236		0.32	0.00	39.09	C
75	4.78	4.49			0.29	0.11	-0.29	26.63	A
	5.62		0.149	0.141		0.15	0.18	37.82	C
124	3.11	2.24			0.87	0.29	-0.02	6.99	A
	2.29		0.029	0.026			0.01	6.43	C
	2.72		0.020	0.016		-0.09	0.13	4.08	C
377	3.93	3.81			0.13	0.26	0.10	3.98	A
	3.80	3.88			-0.08	0.16	-0.07	2.86	A
	3.91		0.034	0.028		0.05	0.01	2.87	C

> 53 MICRON SIZE FRACTION

WT(I)	DRY WT	SI	SI/CI	CA/CI	SR*/SR
0.81	9.1	5.51	1.432	1.095	0.973
0.77	-4.7	4.13	0.919	1.065	0.949
0.45	4.6	3.15	1.403	1.387	0.870
					0.809
0.56	1.4	2.53	0.664	1.033	0.809
			0.652	0.980	

<53 MICRON SIZE FRACTIONS

Z	1-53 MICRON SIZE FRACTION CA	CI	SR	SR*	XS CA	MG	1-53 MICRON FRACTION C_{ORG}	N	C_{ORG}/N	<1 MICRON FRACTION C	N	C/N	CHEM WT	DRY WT	SI(CALC)	SI/CI	CA/CI	SR*/SR	IONS
20	49.5	41.1	0.277	0.207	8.3	6.8	845.	93.1	9.08	162.	14.5	11.20	37.06	51.7	209.2	5.09	1.194	0.748	2.47
20	48.7		0.416	0.346	7.6	6.2	869.	92.5	9.39	182.	16.2	11.25							
75	85.1	75.5	0.496	0.368	9.6	3.7	902.	96.2	9.37	181.	26.9	6.73	42.34	35.6	-96.3	-1.28	1.127	0.741	2.76
124	66.4	64.0	0.455	0.347	2.5	-1.4	344.	42.9	8.01	95.	12.2	7.80	20.47	18.6	-26.7	-0.42	1.038	0.761	8.52
377	68.6	65.8	0.255	0.143	2.8	1.1	176.	15.4	11.39	24.	3.7	6.37	13.02	15.3	32.6	0.50	1.042	0.561	22.85
377		65.8																	

LVFS STATION C115 8 33° 18' S 17° 36' E JAN. 9 1974

Z	CA	CI	SR	SR*	XS CA	MG	K	NA	
20	172.73	73.05			99.68	85.71	13.31	439.21	A
	176.62		3.377	3.252		89.61	11.69	416.62	C
	183.12		3.896	3.772		86.69	37.01	600.21	C
42	56.24	34.18			22.06	20.50	8.16	94.40	A
	62.48		2.340	2.282		20.43	6.95	22.83	C
	54.82		1.986	1.928		20.71	6.60	22.83	C
100	10.64	9.77			0.86	0.36	0.27	47.85	A
	13.14		0.109	0.093		3.18	0.36	76.71	C
150	6.67	5.80			0.87	1.02	0.08	71.67	A
	7.27	6.21			1.06	3.37	0.61	67.55	A
	17.39		0.038	0.028		0.95	0.00	56.84	C
251	17.84	17.49			0.35	1.17	0.43	46.70	A

> 53 MICRON SIZE FRACTION

WT(I)	DRY WT	SI	SI/CI	CA/CI	SR*/SR
198.45	798.7	2721.10	37.249	2.364	0.963
					0.968
113.38	190.4	1565.30	45.788	1.645	0.975
					0.971
12.94	37.5	170.60	17.460	1.088	0.848
2.86	16.6	32.46	5.601	1.150	0.731
			5.226	1.171	
6.52	30.6	68.14	3.896	1.020	-0.145

TABLE 1 (cont.)

LVFS STATION C115 8

Z	CA	1-53 MICRON SIZE FRACTION CI	SR	SR*	XS CA	MG	1-53 MICRON FRACTION C_{ORG}	N	C_{ORG}/N	<1 MICRON FRACTION C	N	C/N	CHEM WT	DRY WT	SI(CALC)	SI/CI	CA/CI	SR*/SR	TONS
20	389.9	290.9	1.482	0.988	99.0	20.0*	19307.	2095.4	9.21	13543.	2199.7	6.16	998.49	1131.5	1900.2	6.53	1.358	0.666	0.31
	400.0		1.853	1.358	109.1	6.7	16793.	1845.1	9.10	10975.	1675.9	6.55							
42	103.5	71.1	1.052	0.931	32.4	16.6	2568.	342.3	7.50	732.	147.8	4.95	115.12	170.7	793.9	11.16	1.456	0.885	1.41
							2533.	297.7	8.51	803.	141.3	5.68							
100	63.4	55.0	0.311	0.218	8.4	16.6	1323.	172.0	7.69	503.	76.6	6.57	64.59	112.9	690.2	12.55	1.153	0.700	2.20
150	151.9	147.2	0.692	0.442	4.7	14.3	1089.	148.2	7.35	123.	20.6	5.98	54.12	105.0	726.9	4.94	1.032	0.638	2.64
251	215.5	192.4	0.642	0.315	23.0	33.1	1368.	190.1	7.20	112.	27.8	4.02	68.32	161.2	1327.0	6.90	1.126	0.491	2.31
	217.8		0.692	0.365	25.4	35.3	1357.	169.1	8.03										

*1 53 μm MG = 87 nmol kg^{-1}

< 1 μm MG = 74 nmol kg^{-1}

> 53 μm size fraction: Nitex mesh, 53 μm mesh opening

CA —calcium
CI —carbonate carbon
SR —strontium
SR* non-carbonate strontium
XS CA —non-carbonate calcium
MG magnesium excess relative to seasalt ratio with sodium
K —potassium excess relative to seasalt ratio with sodium
NA —seasalt sodium concentration in sample

WT(I) —sum of dry weights of carbonate, opal, and celestite
DRY WT gravimetrically determined dry weight (μg kg^{-1})
SI silicate (opal)
SI/CI —opal to carbonate ratio
CA/CI calcium to carbonate ratio
SR*/SR —non-carbonate strontium to total strontium ratio
A —leach by 20% H_3PO_4 + 0.6 N HCl one day
C —leach by 0.6 N HCl one day

1-53 μm size fraction: 'Top glass fiber filter' pore size 1.25 μm at 98% efficiency < 1 μm size fraction: 'Bottom G-F filter' same

C_{org} total carbon less carbonate carbon
N nitrogen
C_{org} N organic carbon to nitrogen ratio
C carbon

CHEM WT sum of dry weights of organic, carbonate, and celestite phases as well as cations (excluding Na) (μg kg^{-1})
SI(CALC) —(dry wt − chem wt)/0.07 (nmol kg^{-1})
TONS —weight of seawater filtered for each sample, metric tons.

KETTEN, BACON and SILKER, 1977; and references therein) indicating that the residence time and hence opportunity for interaction with the water column is greatly reduced.

Five Large Volume *in situ* Filtration System (LVFS) stations were occupied in the Cape Basin of the southeast Atlantic to investigate the relationship among surface biological productivity, particulate distributions, and vertical fluxes. Stations 4, 5, and 8 (Fig. 1) were in areas of high productivity associated with upwelling (HART and CURRIE, 1960); Sta. 7 was within the low productivity South Atlantic central gyre. The aeolian contribution to the particulate matter in the surface waters of the Cape Basin is probably negligible (CHESTER, ELDERFIELD, GRIFFIN, JOHNSON and PADGHAM, 1972; KRISHNASWAMI and SARIN, 1976).

The hydrographic, biological, and particulate mass and elemental distributions (Na, Mg, Ca, K, Sr, Si, carbonate, C, and N) at these stations are presented to expand the results of BISHOP *et al.* (1977). The size distributions of Foraminifera, fecal pellets, and fecal matter in the samples from 400 m at Stas. 5, 6, and 7 together with the chemical data and two mass flux models are used to calculate the composition and magnitude of the particle flux as a function of biological productivity.

METHODS

BISHOP and EDMOND (1976) have discussed in detail the LVFS, its calibrations, filtration sequence, and filter handling technique. Methods of analysis of LVFS samples are given by BISHOP *et al.* (1977). The particulate data and locations of LVFS Stas. 4 to 8 are listed in Table 1.

Hydrographic data were obtained using the methods of CARPENTER (1965), O_2; MULLIN and RILEY (1955), reactive Si; and MURPHY and RILEY (1962), PO_4. Salinity was measured at Woods Hole on stored samples (6 months). Temperature and depth were determined by standard thermometric techniques. The data are listed in BISHOP (1977).

RESULTS AND DISCUSSION

The hydrography of the Southwest African continental margin has been studied by numerous workers (HART and CURRIE, 1960; DE DECKER, 1970; CALVERT and PRICE, 1971; JONES, 1971; BANG, 1971; BANG and ANDREWS, 1974). Temporal and spatial variability is characteristic of the area (BANG, 1971, 1973; BANG and ANDREWS, 1974); therefore, a hydrographic survey was necessary to characterize the LVFS stations.

Closely spaced bathythermograph profiles showed a weakly developed mixed layer to 15 or 20 m at Sta. 4; near Sta. 8, there were strong horizontal temperature gradients (8°C over 30 km) and there was no mixed layer. The mixed layer was developed to 30, 50, and 65 m at LVFS Stas. 5, 6, and 7. All stations exhibited a weak salinity maximum in the upper thermocline and those between Stas. 4 and 5 showed considerable structure in all hydrographic properties (Fig. 2).

HART and CURRIE (1960) described a northward-flowing surface current near the coast (Benguela Current), a subsurface poleward compensation current at the shelf edge, a general onshore transport of water from depths of several hundred meters, and upwelling near the coast or at the shelf edge with offshore transport of the surface water. This scheme results in nutrient enrichment of the coastal waters by a mechanism similar to that for estuaries (HART and CURRIE, 1960; CALVERT and PRICE, 1971) and is responsible for the distribution anomalies of Si, PO_4, and O_2 relative to their offshore salinity relationships (Fig. 3). During

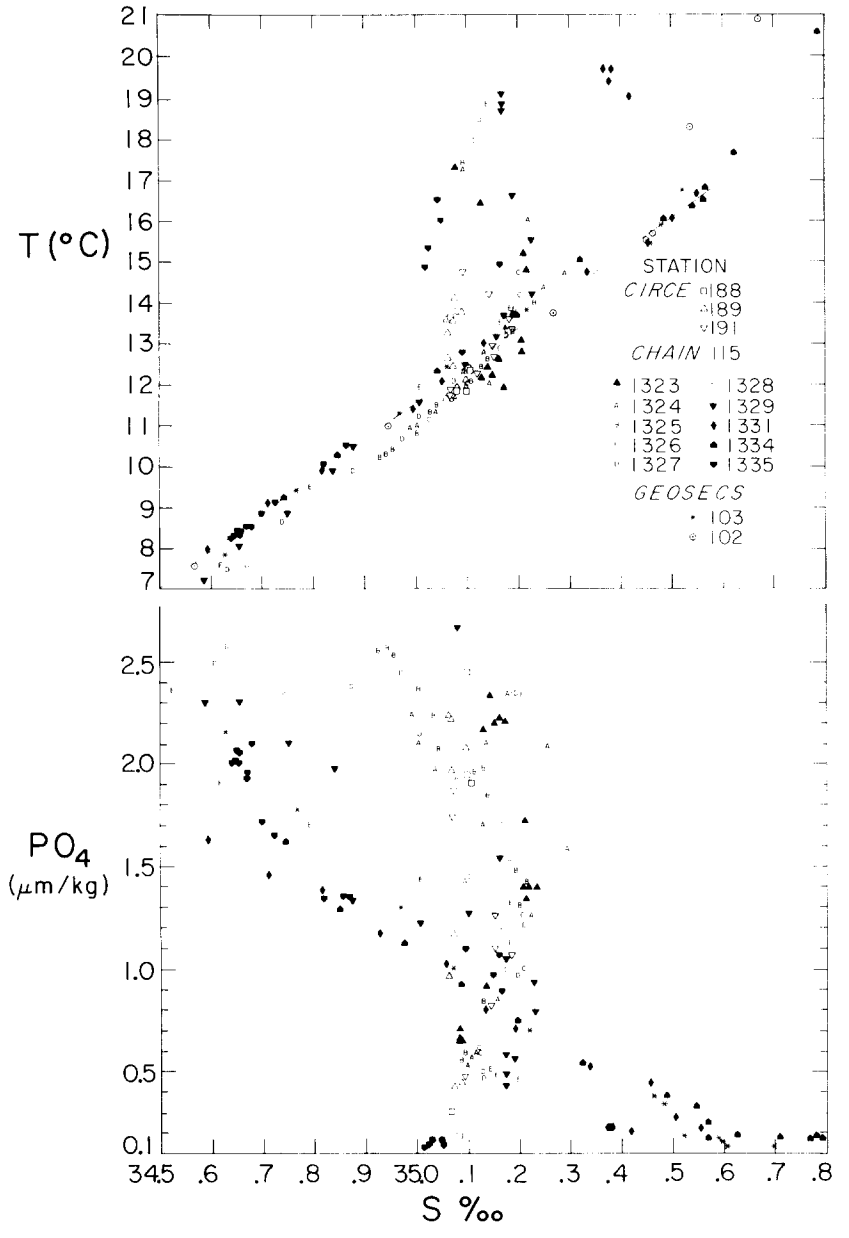

Fig. 3. T–S and PO_4–S plots for the shallowest 500 m at all stations in the Cape Basin including some results from the CIRCE and GEOSECS expeditions. The line drawn through the T–S data is the best fit of the data from hydrostations 1331 and 1334 (LVFS Stas. 6 and 7) for water colder than 17°C. It is apparent that the near-bottom water on the shelf has not come from immediately offshore. Nearshore stations plot vertically on the PO_4–S diagram, indicating intense regeneration of organic matter. O_2–S and Si–S relationships are similar with values ranging from 300 to 10 μmol O_2 kg^{-1} and 2 to 25 μmol Si kg^{-1}, respectively (at 35.1‰S, surface to 180 m, LVFS Sta. 4).

active upwelling, driven by the local winds, the onshore–offshore circulation is accelerated. During quiescence, the circulation is sluggish and intense regeneration of organic matter rapidly consumes oxygen in the shelf water producing the mortalities commonly associated with such conditions (DE DECKER, 1970).

The poleward compensation current is identified by a nearly isothermal oxygen-poor layer (BANG, 1973; DE DECKER, 1970) and anomalous T–S properties. The data show such a layer at 300 m on the shelf with T–S properties either cooler or more saline than the immediate offshore waters (Fig. 3). The data of the CIRCE Expedition (Oct. 1968) indicate that this layer has an offshore origin 100 km to the north. The strongest nutrient and O_2 anomalies were in this layer and decreased westward. The 120-m sample at LVFS Sta. 5 could be a remnant of this deep coastal water (Fig. 2).

LVFS Sta. 4 was typical of quiescent upwelling conditions. The 18°C surface water had 0.7 μmol kg^{-1} PO_4 and 2.5 μmol kg^{-1} Si, was intensely green and highly productive (visivility <2 m). Waters at LVFS Sta. 5 were greenish and allowed 10 m of visibility. Those of Stas. 6 and 7 were more typical of open ocean conditions.

Upwelling was active at Sta. 8 and typical for this season (JONES, 1971; BANG, 1971; BANG and ANDREWS, 1974). Surface waters were opaque green and extremely productive.

Table 2. > 53-μm *organism distributions* (*No./*l).

Z	FORAMS	PT?	A.RAD	J.RAD	C.DIA	S.DIA	P.DIA	G.DIA	SIFLAG	ACANT	TINT	DINOFL
Station 4												
20	30.78		1.52	3.04	22.04	12.54	3.42	4.18	11.02	3.80	1.52	4.18
42	8.96		12.67	3.54	5.49	8.02	1.30	.61	3.97	1.23	1.52	.25
100	4.42		4.87	2.58	3.66	1.13	.31	.40	.60	.48	.88	
183	3.60		1.53	.38	8.24	3.16	.48	.82	.48	.10	.14	.10
Station 5												
20	44.71		2.65	0.09	179.04	37.14	.27	.37	4.84	33.49	.46	3.28
40	34.59	.70	2.16	0.23	463.75	24.38	.88	.23	4.84	21.12	1.28	12.60
50	20.60	.06	9.64	0.46	45.58	15.72	.28	1.23	44.68	2.13	2.32	.56
88	7.02	.02	2.73	1.47	25.14	21.06	.23	.48	4.91	.80	.73	.87
124	5.60	.02	6.98	2.04	10.41	3.06	.02	.80	2.19	.83	1.59	.06
199	2.90	.10	4.10	1.10	3.13	1.36	.60	.14	1.05	.26	.76	.01
292	2.70		4.20	0.70	1.67	.49		.14	.80	.20	.74	
379	1.54		4.64	1.05	2.34	1.71		.01	.98	.13	.45	
Station 6												
26	13.21	.09	1.75	0.00	1.56	1.79	.05	.05	2.03	30.67	.09	2.12
52	29.20	.53	2.33	0.05	35.56	113.42	1.06	.53	12.19	7.10	.15	.53
113	6.21	.09	2.54	0.36	16.67	.50	9.94	.46	5.67	.96	.81	.13
187	1.80	.02	2.18	0.41	2.00	.04	.26	.03	3.26	.66	.08	.03
289	1.75	.01	1.95	0.14	.77	.21	.34	.05	.61	.23	.03	
386	1.16	.04	1.79	0.18	.97	.10	.30	.04	.72	.23	.04	
Station 7												
20	2.31		0.78	0.00	.37	.23	.60	.41	14.52	3.91	.18	1.38
75	2.75		2.69	0.03	.40	2.32	.43	.16	17.38	1.14	.03	.19
124	2.21		1.47	0.03	1.22	2.12	.35	.13	7.28	.06	1.25	.16
377	.29		0.93	0.05	.17	.45	.02	.01	.41	.03	.04	
Station 8												
20	23.61		11.81	1.07	11414.90	870.47	4.29	1.07	640.78	10.73		148.12
42	6.80		4.67	1.01	4430.80	185.50	7789.15		36.33	6.29	0.61	26.03
100	3.96		37.52	5.05	137.70	32.16	18.10	4.20	13.13	.47	2.87	3.34
150	.93		5.56	2.78	6.81	5.99	1.09	1.14	.65		.22	.11
251	.82		3.59	0.65	6.69	1.88	.92	.41	.41		.41	.16

Z—depth (m)
FORAMS—Foraminifera
PT?—pteropods (?)
A. RAD—adult Radiolaria
J. RAD—juvenile Radiolaria
C. DIA—centrate diatoms
S. DIA—solenoid diatoms
P. DIA—pennate diatoms
G. DIA—gonioid diatoms
SIFLAG—silicoflagellates
ACANT—Acantharia
TINT—tintinnids
DINOFL—dinoflagellates.

Whole organisms only; blanks in the data indicate organisms not present on subsample analysed.

Biological distributions

The LVFS samples are suited for determining the quantitative vertical distributions of non-motile organisms. The data (Table 2) are valuable in understanding the chemical distributions in the samples.

A common feature of all stations was the strong vertical gradient in organism abundance within the upper 100 m. The largest number of intact, live organisms was found in the near-surface samples and concentrations decreased rapidly with depth due to predation and dissolution.

Of the Walvis Bay section (LVFS Stas. 4 to 7), Sta. 5 had the highest populations of Foraminifera, Acantharia, diatoms, silicoflagellates, tintinnids, and dinoflagellates. Station 4

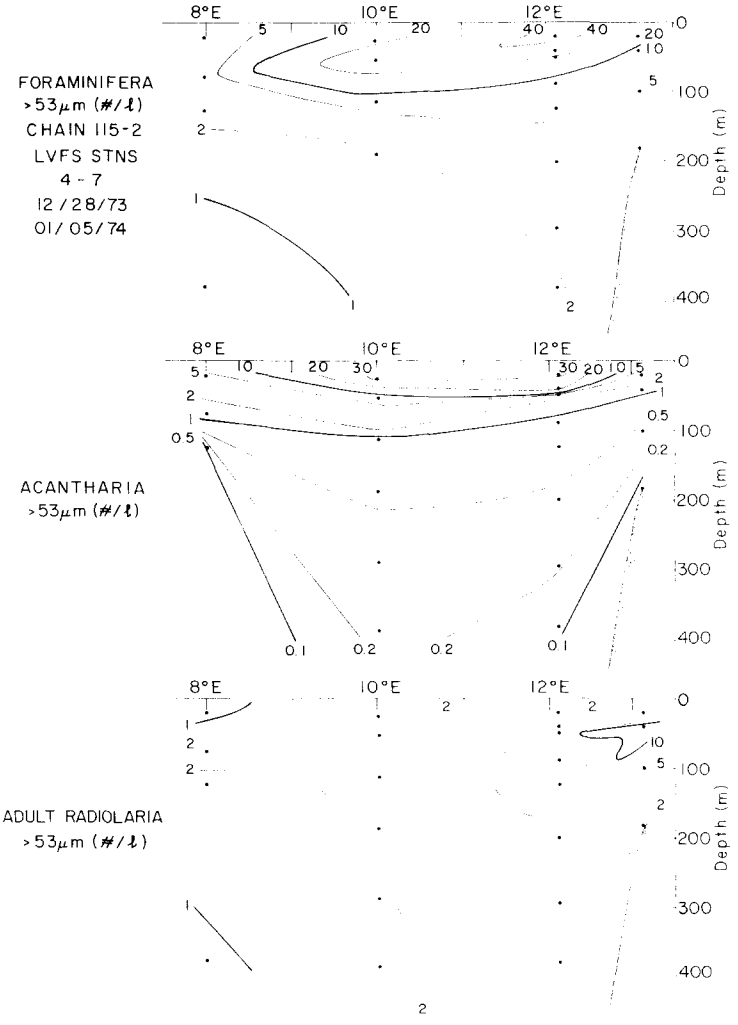

Fig. 4. Distributions of Foraminifera, Acantharia, and Radiolaria for LVFS Stas. 4 to 7, >53-μm size fraction. Strong vertical gradients of organisms necessitated the use of a logarithmic contouring interval.

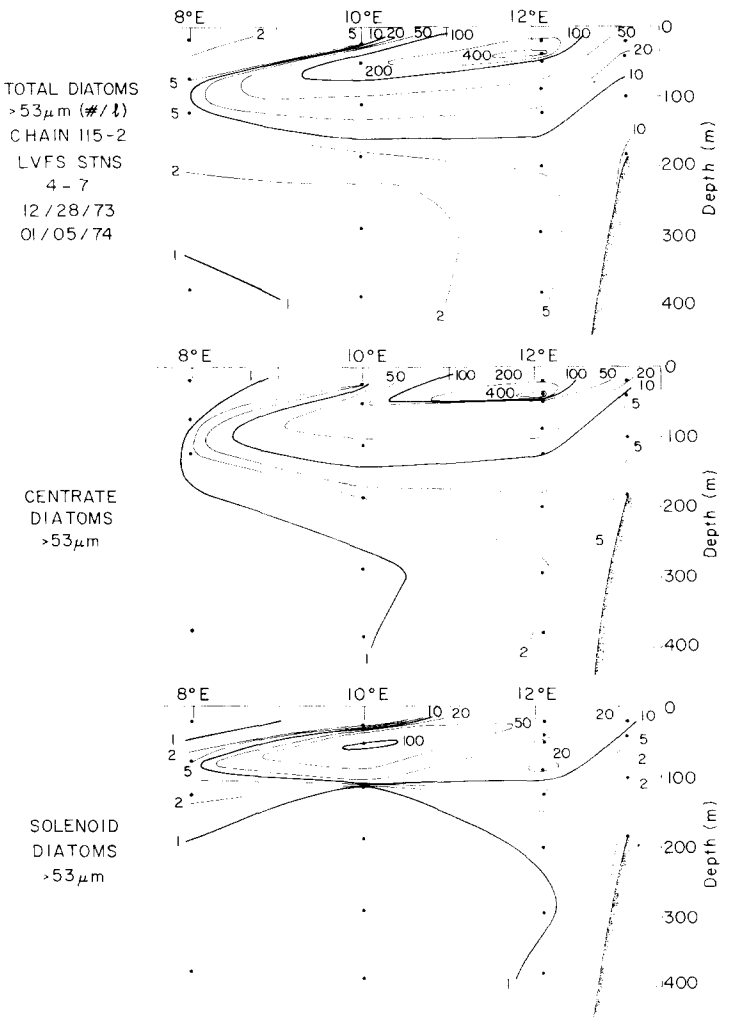

Fig. 5. Distributions of total Diatomaceae and centrate and solenoid diatoms at LVFS Stas. 4 to 7, > 53-μm fraction. These organisms have maxima near the base of the mixed layer.

had the maximum population of Radiolaria; Sta. 6 showed a strong maximum of solenoid diatoms, primarily species of Rhizosoleniaceae. Coccolithophorids dominated both the > 53- and < 53-μm size fractions at Sta. 4.

Acantharia, Foraminifera, and Radiolaria exhibited contrasting vertical distributions (Fig. 4). Acantharia had a surface maximum at all stations and were most abundant at Stas. 5 and 6. Foraminifera density maxima occurred nearest the surface at Stas. 4 and 5 and near the base of the mixed layer at Stas. 6 and 7. Organisms with reduced conical of planospiral carbonate shells larger than 100 μm in diameter, tentatively identified as pteropods, had maxima at the base of the mixed layer at Stas. 5 and 6. Adult and juvenile Radiolaria were primarily in the upper thermocline, deeper than most other organisms. Similar vertical distribution trends have been obtained by BERGER (1968) and PETRUSHEVSKAYA (1971) for Foraminifera and Radiolaria, respectively. In spite of contrasting methods, the agreement of

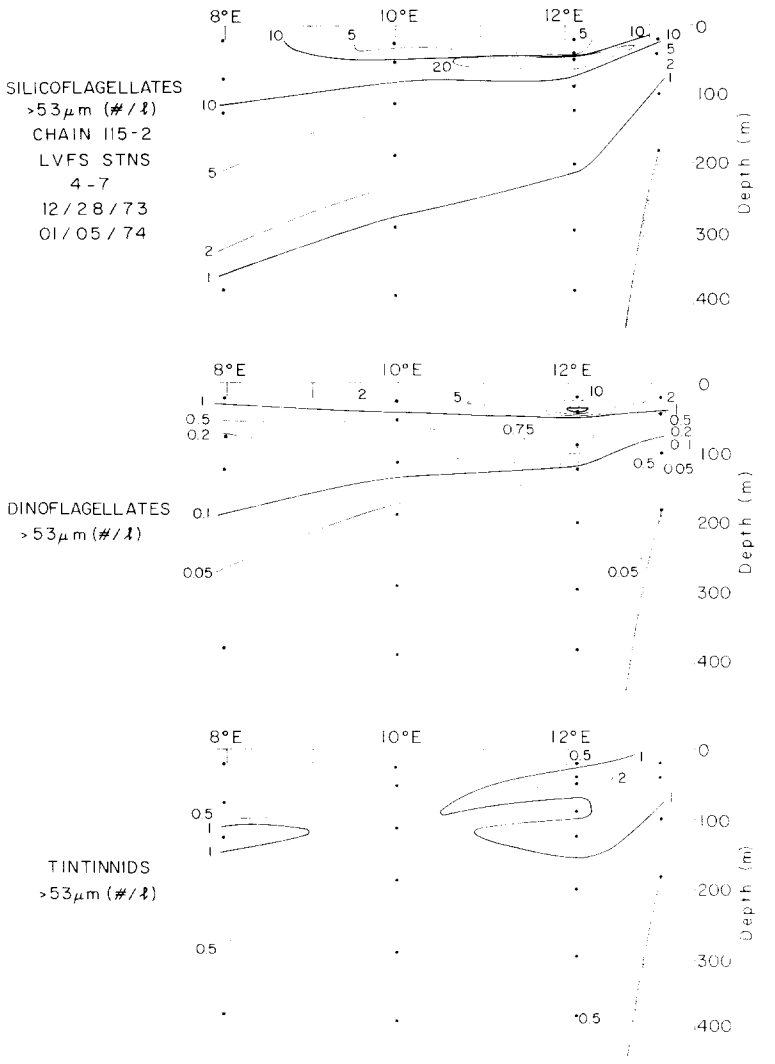

Fig. 6. Distributions of silicoflagellates, dinoflagellates, and tintinnids at LVFS Stas. 4 to 7, >53-μm size fraction.

their data with those of the LVFS suggests that the occurrence of Radiolaria deeper than Foraminifera is a general phenomenon.

Diatoms (Fig. 5) were densest near the surface at Sta. 4 and near the base of the mixed layer at Stas. 5, 6, and 7. Centrate and solenoid diatoms were most significant contributors to the >53-μm diatom counts. Centrate diatoms dominated at Stas. 4 and 5, whereas solenoid diatoms dominated at Stas. 6 and 7.

Silicoflagellates (Fig. 6) had maxima nearest the surface at Sta. 4, in the upper thermocline at Sta. 5, and near the base of the mixed layer at Stas. 6 and 7. The distribution of dinoflagellates reflects both their fragility and light requirements as they were generally nearest the surface. Tintinnids were distributed similarly to Radiolaria.

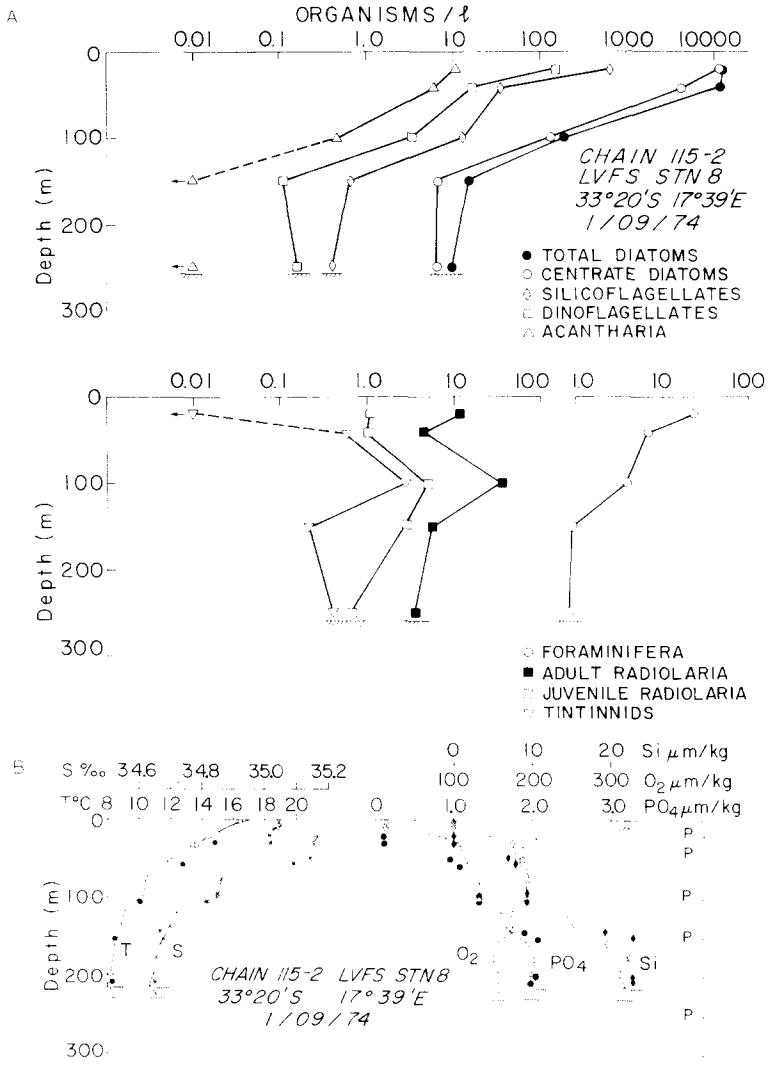

Fig. 7. (A) Distributions of organisms at LVFS Sta. 8 near Cape Town. '←' indicates an extrapolation for organisms not encountered in the subsample studied. > 53-μm size fraction. (B) Hydrographic data for Sta. 8 demonstrating a 20-m excursion for most properties over a period of several hours. 'P' indicates the depths at which the LVFS was operated.

Station 8 had similar vertical distribution patterns of all organisms but different relative abundances compared to the Walvis Bay stations (Fig. 7). Diatoms were most significant contributors to the biomass.

The fall (March, 1950) data of Hart and Currie are most comparable to those of the LVFS stations near Walvis Bay. These authors found 10 to 100 × 10^6 diatoms per vertical haul of a 44-μm mesh, 0.5-m net at Stas. WS 979 to 981. A minimum diatom concentration of 5000 l^{-1} can be calculated assuming a 10 m^3 volume filtered and a catch of 50 × 10^6 diatoms by their net. The concentration is two orders of magnitude higher than observed at LVFS Sta. 4. There were ~ 5000 l^{-1} coccolithophorids > 50 μm in size, in marked contrast to the few

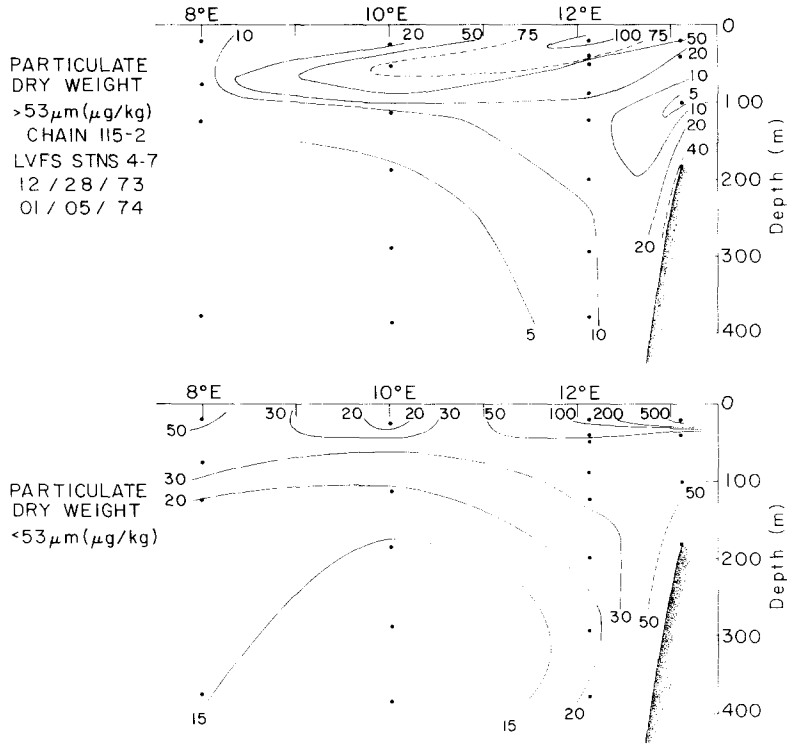

Fig. 8. >53-μm and <53-μm particulate dry weight sections for LVFS Stas. 4 to 7. >53-μm distribution reflects the organism distributions.

observed by HART and CURRIE (1960). The diatom distributions at Sta. 8 were comparable.

The deep scattering layer (DSL), as observed by a 12-kHz Precision Graphics Recorder, migrated surfaceward at sunset from the bottom and near bottom at Stas. 4 and 8, and from 400, 450, and 400 m at Stas. 5, 6, and 7. Sonic backscattering from this layer was weakest at Sta. 7, indicating a sparse population of DSL organisms.

The high productivity at Sta. 4 was due almost entirely to coccolithophorids; only at Stas. 5 and 6 were diatoms significant contributors to the >53-μm fraction. Station 7 was sparsely populated with plankton. Station 8 was the only station where upwelling was active.

Dry weight

BISHOP and EDMOND (1976) found systematic differences between LVFS and 30-l. Niskin dry weight profiles. Recent work by GARDNER (1977) and our microscopic observations give improved explanation for the discrepancy between the two techniques. Since the Nuclepore filters have been analysed for Si, it is necessary to understand the biases of the Niskin data.

The >53-μm dry weight distribution reflects the organism abundances (Fig. 8). Maxima were nearest the surface at Stas. 4 and 5 and near the base of the mixed layer at Sta. 6. The intense maximum at Sta. 8 reflects the high productivity. The subsurface minimum at Sta. 4 was lower than at Sta. 5, indicating a relatively small concentration of sinking material.

The <53-μm dry weight distributions had maxima nearest the surface at Stas. 4, 5, 7, and 8 and at the base of the mixed layer at Sta. 6. High concentrations at Stas. 4 and 8 reflected their high productivity.

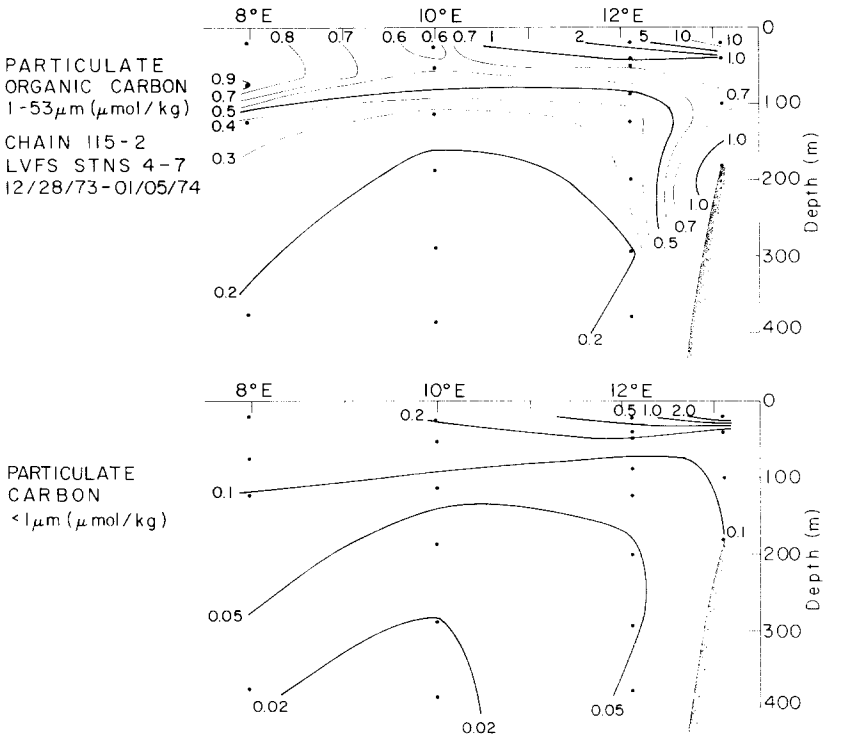

Fig. 9. 1- to 53-μm and < 1-μm particulate organic carbon distributions at LVFS Stas. 4 to 7.

The particulate mass distributions determined by LVFS and Niskin methods show poorest agreement at stations where the > 53-μm material was a substantial fraction of the total mass. In these cases, organisms were large and numerous and particularly prone to settling to the bottom of the Niskin sampler and thus not filterable. This kind of loss has been shown to be as high as 50% by GARDNER (1977). The agreement of the LVFS and Niskin methods should be best at stations where most particles are small or sink slowly; i.e. Sta. 4. The Geochemical Ocean Sections (GEOSECS) particulate data (BREWER, SPENCER, BISCAYE, HANLEY, SACHS, SMITH, KADAR and FREDERICKS, 1976) agree to within 30% with the LVFS data for the depth interval 100 to 400 m.

Organic carbon and nitrogen

MENZEL (1974) argued that the current particulate organic carbon data fail to demonstrate spatial or time variability for samples below 200 m. Recent values for this deeper water seldom exceed 0.8 μmol (10 μg) C kg^{-1}.

GORDON (1971) found scattered particulate carbon values (1.2-μm Ag filters) averaging 0.3 μmol C kg^{-1} for the 200- to 500-m depth interval in the tropical North Pacific. Similar samples (0.8-μm Ag filters) from the Atlantic between Halifax and Bermuda gave values of 0.5 μmol C kg^{-1} (GORDON, 1977). The 0.1 μmol C kg^{-1} error for these samples made interpretation of individual profiles difficult. Gordon's statistical analysis of his data did show a systematic decrease in particulate carbon concentrations with both depth and overlying surface productivity. Gordon's samples were not treated to remove carbonate prior to analysis.

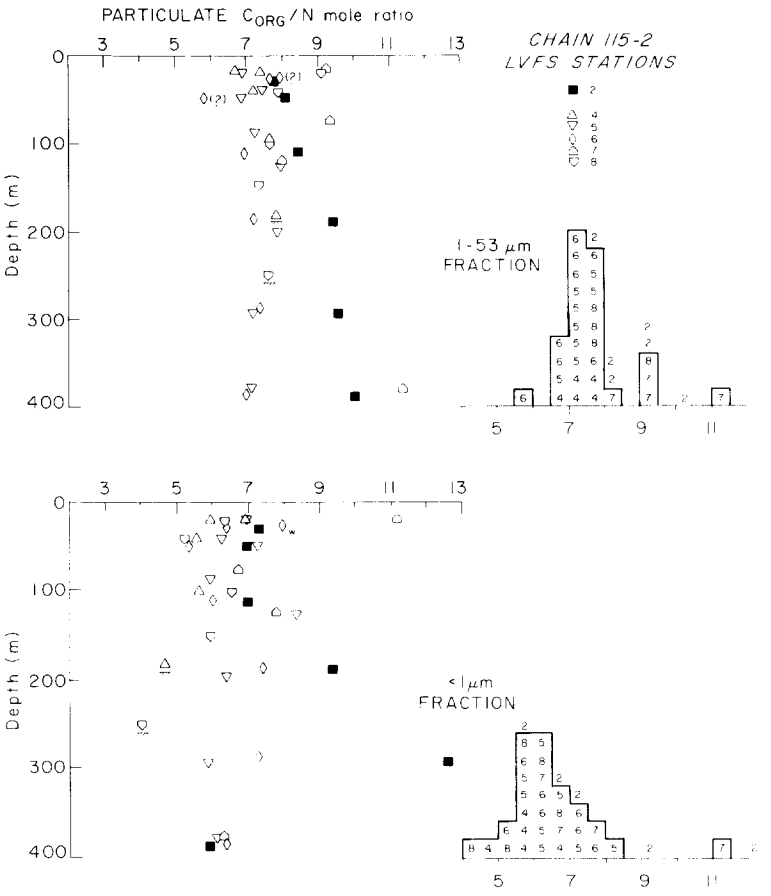

Fig. 10. Particulate organic C/N ratios in the 1 to 53 and < 1-μm size fractions. The data for Stas. 4, 5, 6, and 8 are rather uniform with depth, contrasting with Stas. 2 and 7. The < 1-μm fraction is consistently N enriched, perhaps indicating the presence of bacteria.

HOBSON and MENZEL (1969) found values (1.2-μm Ag filters) of 0.2 to 1.0 μmol C kg^{-1} for 200- to 500-m samples from the tropical southwest Atlantic. WANGERSKY (1976) reported values (0.8-μm Ag filters) averaging 1.4 μmol C kg^{-1} for 100 to 500 m (*Hudson* 70, 0 to 30° S, 30°W). For comparison, BREWER *et al.* (1976) found total particulate mass concentrations averaging 11.9 μg kg^{-1} for GEOSECS samples from the same depth interval and region of the South Atlantic. These two data sets conflict although SHELDON (1972) and FEELY (1975) have stated that glass and silver filters are more efficient than Nuclepore filters for retaining smaller particles.

Particulate organic carbon maxima (Fig. 9) occur near the surface at LVFS Stas. 4 and 5 and near the base of the mixed layer at Stas. 6 and 7. Concentrations decrease regularly with depth at all stations and values fall below 0.3 μmol C kg^{-1} for samples deeper than 200 m. Higher values at Sta. 8 reflect active upwelling. The < 1-μm particulate carbon accounts for 25 and 50% of the near-surface < 53 μm particulate carbon at Stas. 4 and 8.

The particulate organic carbon and nitrogen distributions are similar, with nitrogen being lower by a factor of 7 (Fig. 10). The 1- to 53-μm C_{org}/N ratios at Stas. 4 to 6 are remarkably

uniform at 7.3 ± 0.5 (σ), in agreement with HOBSON's (1971) surface values for the same region. Station 8 has a surface maximum but other values are similar to those at Stas. 4 to 6. Only Sta. 7 shows an increase of C_{org}/N ratio with depth similar to that of Sta. 2.

BISHOP *et al.* (1977) suggested that nitrogen-rich marine bacteria could account for a substantial fraction of the < 1-μm organic material, especially in the near-surface waters. This seems to be substantiated by the data from Stas. 4 to 8 as the < 1-μm fraction is consistently nitrogen rich relative to the 1- to 53-μm material.

The concentrations of particulate organic matter below the euphotic zone depend upon surface productivity. Variations are such that they are undetectable by conventional methods. Both GORDON (1977) and the LVFS results provide evidence contrary to MENZEL's (1974) hypothesis that particulate organic matter is distributed uniformly in space below 200 m.

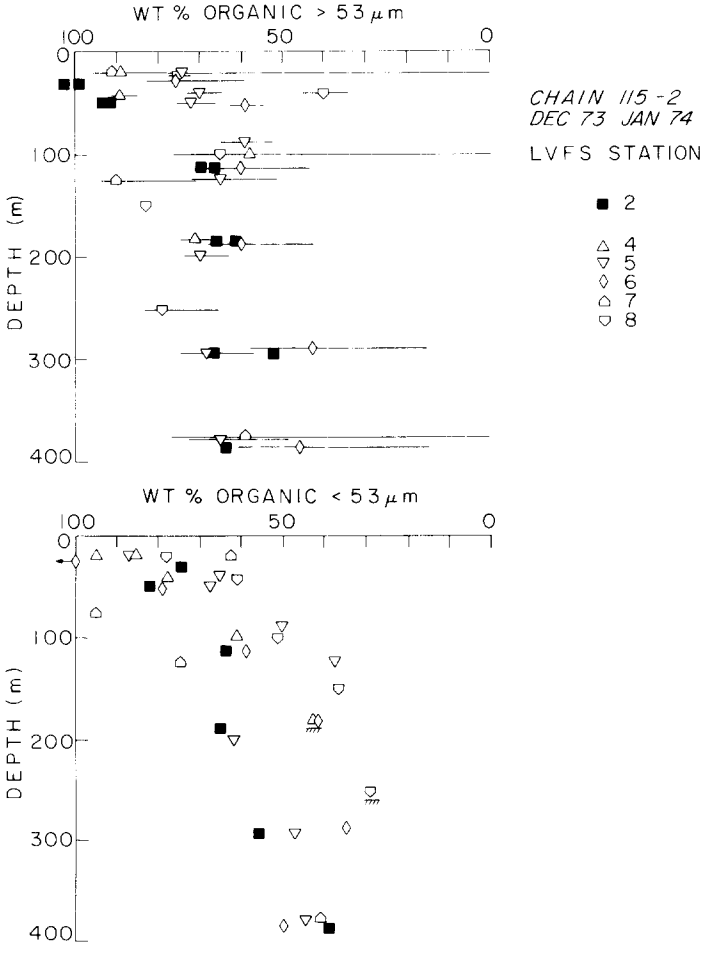

Fig. 11. Percentage of particulate dry weight attributable to organic matter (calculated as 'CH_2O + N' for the < 53-μm fractions and as 'total dry weight − (carbonate + opal + celestite)' for the > 53-μm fraction). The large error bars in the > 53-μm fraction values are due to the uncertainty in dry weight values. The > 53- and < 53-μm material at 400 m is 60 and 50% organic compared with nearly 100% at the surface.

The similarity of the sections for < 53-μm dry weight C_{org} and N indicates the important contribution of organic matter to total dry weight. Nearly 100% of the material near the surface is organic (Fig. 11). Preferential destruction of organic material results in 50 and 60% values for the < 53- and > 53-μm fractions in the deeper samples. The < 53-μm near-bottom samples at Stas. 4 and 8 are more depleted in organic material, indicating resuspended bottom material.

The striking feature of the organismal, dry weight, and organic carbon and nitrogen distributions at all stations is the strong vertical concentration gradient within the upper 100 m. This feature can only be maintained by grazing organisms feeding on the phytoplankton and microzooplankton populations found in the euphotic zone. The LVFS data show that the discrepancy between conventional particulate carbon and dry weight measurements lies with the particulate carbon technique.

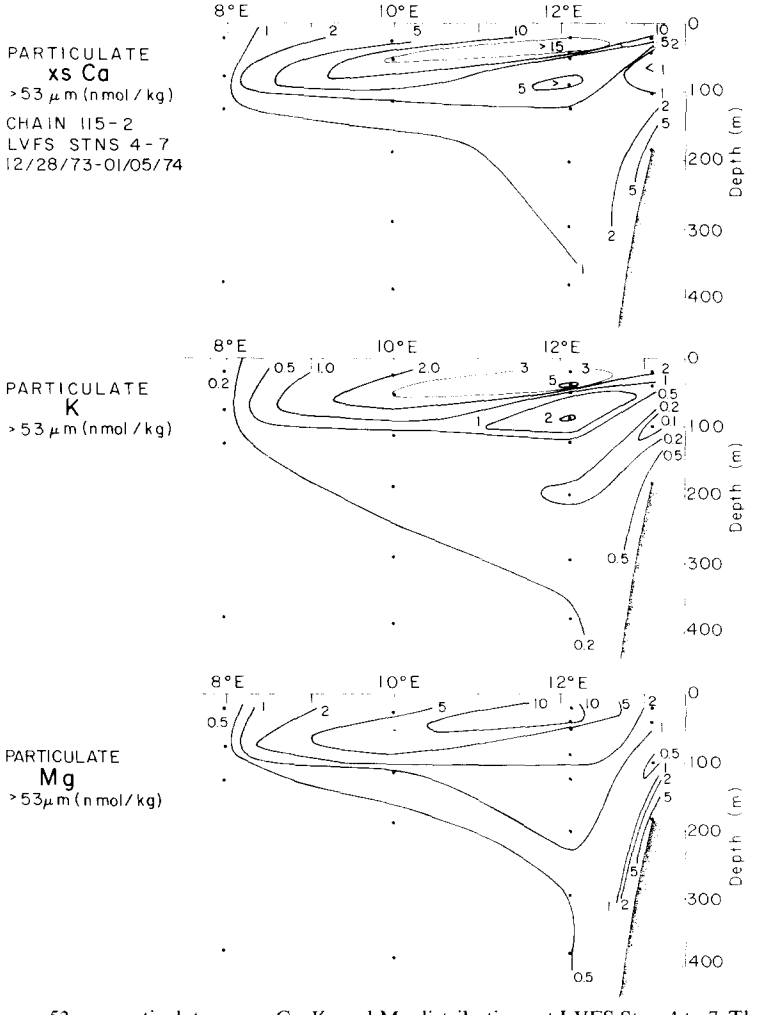

Fig. 12. > 53-μm particulate excess Ca, K, and Mg distributions at LVFS Stas. 4 to 7. The overall features of the distributions are similar to those of the organisms; excess Ca and K covary similarly, contrasting with Mg.

Excess major ions: Ca, K, *and* Mg

BISHOP *et al.* (1977) showed that Ca, K, and Mg were associated with organic matter at ion-exchangeable or complexing sites. These elements are present in the cytoplasm of phytoplankton (MAYZAUD and MARTIN, 1975) and are biochemically significant (HUGHES, 1972). The importance of the organic fraction as a carrier of minor and trace elements to the deep ocean is demonstrated by the presence of Sr at ion-exchangeable organic positions (BISHOP *et al.*, 1977) and by the correlations of dissolved Cd and Ni with phosphate (BOYLE, SCLATER and EDMOND, 1976; BENDER and GAGNER, 1976; SCLATER, BOYLE and EDMOND, 1976).

The > 53-μm excess Ca, K, Mg, and dry weight distributions have grossly similar features (Figs. 12 and 8). Estimated C_{org}/excess-Ca and C_{org}/Mg ratios are 100 to 200 for near-surface samples, comparable with those of Sta. 2. The details of the excess-Ca and K sections are the same, differing from those of Mg. Below 100 m excess-Ca and K occur in significant quantities relative to Mg at Stas. 4, 5, and 8, contrasting with relative depletions at Stas. 6 and 7. Excess Ca and K are involved in shallow regenerative cycles and are present in deep samples only in areas of high productivity.

The 1- to 53-μm excess-Ca and Mg data (Table 1) show near-surface maxima at Stas. 4, 5, 7, and 8. Secondary maxima occur near bottom at Sta. 4 and at 50 m (Mg) and 124 m (Ca) at Sta. 5. Two near-surface samples at Sta. 6 gave negative Mg values using the calculation scheme of BISHOP *et al.* (1977). This is explained by preferential dissolution of sea salt Mg

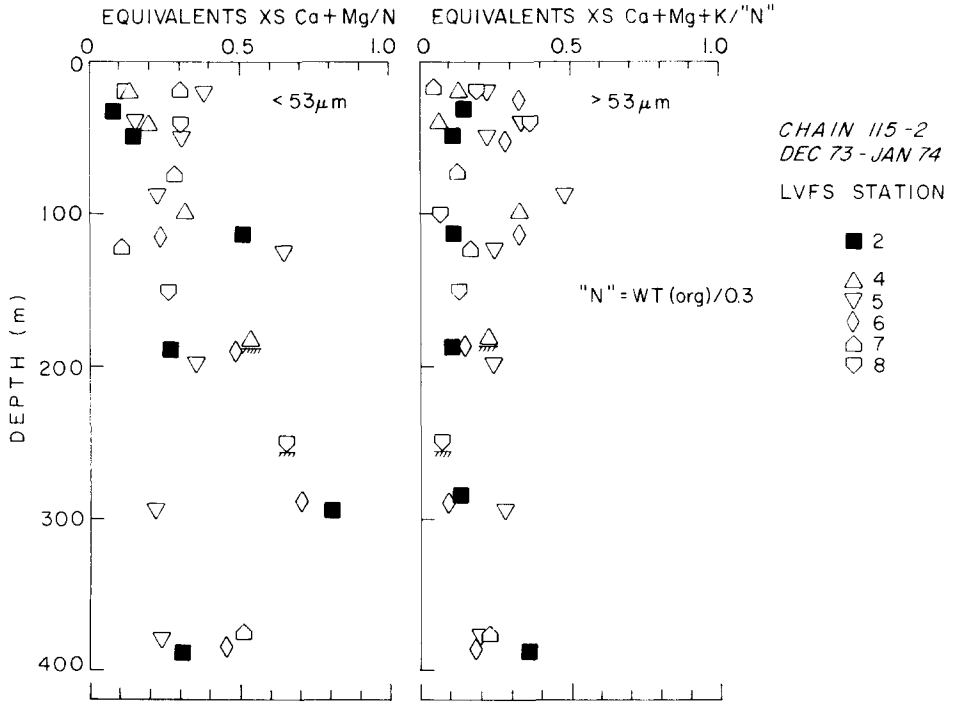

Fig. 13. > 53- and < 53-μm particulate excess cation charge to nitrogen ratio for LVFS Stas. 2 and 4 to 8. The value of the ratio is equivalent to the fractional reduction of the alkalinity effect proposed by BREWER *et al.* (1975), assuming that cations occupy negative sites on organic matter.

relative to Na after the two samples were rewashed with distilled water in the laboratory. The 'bottom' glass fiber filter from 20 m at Sta. 8 had twice the magnesium content of similar filters from other samples. It is assumed that this Mg is particulate and so < 1-μm and 1- to 53-μm values are reported for this sample. With the exception of Sta. 6, the C_{org}/Mg ratio for near-surface samples is 100 to 200.

The ratio of total equivalents of cations to nitrogen (Fig. 13) is a measure of the reduction of the proposed effect upon seawater alkalinity produced by the oxidation of organic nitrogen (BREWER, WONG, BACON and SPENCER, 1975). The cation charge to nitrogen ratio for the > 53- and < 53-μm fractions is 0.22 for samples shallower than 100 m; deeper samples show no change for the > 53-μm fraction but increase to values averaging 0.4 for the < 53-μm fraction, essentially the same as at Sta. 2. The proposed decrease in alkalinity due to organic matter oxidation is compensated at least 20% by cations occupying negative sites on the organic particles. The role of anions in the charge balance of plankton and particulate matter is unknown.

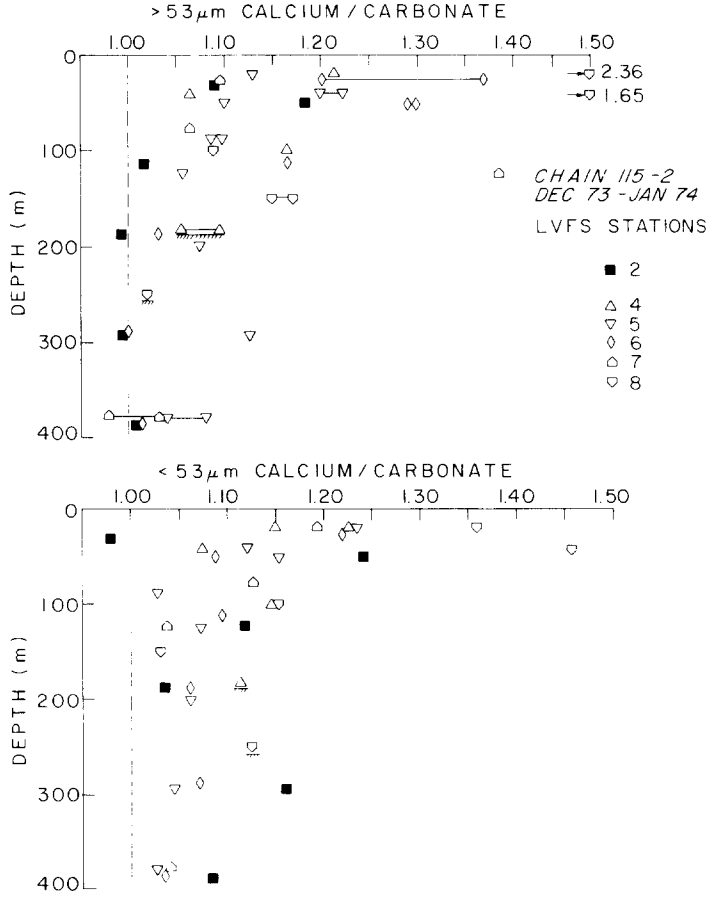

Fig. 14. > 53- and < 53-μm particulate Ca to carbonate ratios at LVFS Stas. 2 and 4 to 8. Values exceeding 1.5 were found in the upper 50 m at Sta. 8, where diatoms dominated the population. The organic carbon to excess calcium ratio fell in the range 100 to 200 : 1.

Calcium and carbonate

BREWER *et al.* (1975) argued that calcium is a better tracer than alkalinity for carbonate dissolution. The profiles of particulate Ca/carbonate ratios (Fig. 14) for both size fractions demonstrate that calcium is involved in cycles other than that of precipitation and dissolution of calcium carbonate.

The >53-μm samples shallower than 100 m at Stas. 4, 5, and 6 (and 2) had Ca/carbonate values averaging 1.25; at Sta. 7, 1.10; and at Sta. 8, 2.0. Deeper samples at Stas. 4, 5, and 8 had values of 1.07; those at Stas. 6 and 7 were 1.00.

Ratios fell between 1.10 and 1.20 for most <53-μm samples shallower than 100 m. The exception was at Sta. 8 where values exceeded 1.4. Deeper samples averaged 1.07.

The interpretation of particulate Ca as calcium carbonate can give errors especially in high productivity areas where diatoms predominate. If we assume that C_{org}/excess-Ca in primary producers is 200 (a minimum estimate) and that the yearly productivity of the oceans is 23×10^9 tons C yr^{-1} (KOBLENTZ-MISHKE, VOLKOVINSKY and KABANOVA, 1970); then 10^{13} mol of Ca are fixed in the tissue of plankton each year. Total calcium carbonate precipitation by organisms was estimated as $7 \pm 2 \times 10^{13}$ mol yr^{-1} (LI, TAKAHASHI and BROECKER, 1969). Therefore the removal of calcium and carbonate from the mixed layer is in the ratio 1.13 to 1.2 and could be as high as 1.4 if a C_{org}/excess-Ca value of 100 is used. This invalidates the use of surface seawater as a reference for carbonate dissolution as was done by BREWER *et al.* (1975).

Carbonate

Most particulate carbonate is produced by coccolithophorids and Foraminifera. The near-surface carbonate distribution resembles that of Foraminifera (Figs. 15 and 4); these distributions differ in the deeper samples. Plots of >53-μm carbonate/Foraminifera (Fig. 16) show that coccolith enrichment of the large particles with depth is a general feature of the particulate matter in the southeast Atlantic. The high ratio at 88 m at Sta. 5 is the only instance where Foraminifera made an appreciable contribution to total carbonate. The near-bottom samples at Stas. 4 and 8 have high ratios indicating strong enrichment with coccoliths. The general increase with depth of the >53-μm carbonate/Foraminifera ratio must be the result of large particle grazing by detritovores.

Stations 4, 5, and 8 have near-surface maxima of <53-μm carbonate (Fig. 15, Table 1). Replicate samples at Sta. 4 had concentrations of 470 and 370 nmol kg^{-1} and coccolithophorid populations of 6200 and 4400 l^{-1}, respectively. These data allow the calculation of $\sim 7 \times 10^{-2}$ nmol carbonate per coccolithophorid, approximately 45 times the values for open ocean coccolithophorids (HONJO, 1976). Sta. 4 coccolithophorids were ~50 μm in size compared to 10 to 20 μm at the other stations. Station 5 exhibited an unusual distribution where coccospheres at 20 and 40 m, coccoliths at 50 m, and a mixture of coccospheres and coccoliths at 88 m determine the <53-μm carbonate. Coccoliths dominate all samples below 100 m.

The spatial variability of the <53-μm carbonate in deeper samples is noteworthy. The low at 100 m at Sta. 4 and the high at 88 and 124 m at Sta. 5 may be due to lateral advection of water. Uniform concentrations of 66 ± 1.4 (σ) nmol kg^{-1} are found for five samples at Stas. 6 and 7. These values are twice those at Sta. 2, indicating significant spatial variability in carbonate distribution. Near-bottom maxima at Stas. 4 and 8 are due to resuspended sediments.

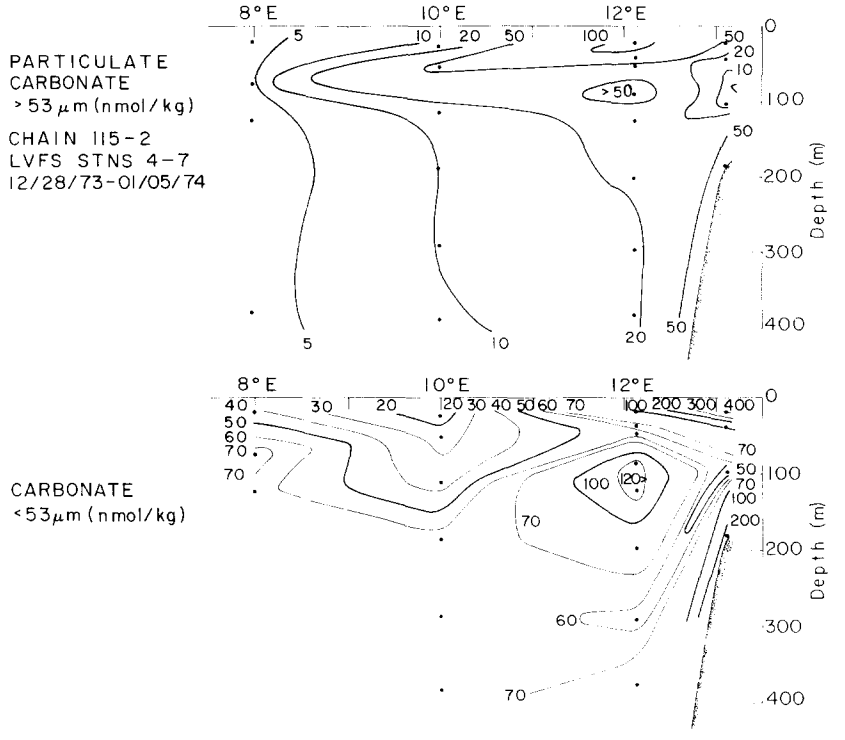

Fig. 15. >53- and <53-μm particulate carbonate distributions at LVFS Stas. 4 to 7. In the upper 100 m a large fraction of the >53-μm carbonate was due to foraminifer. Coccoliths dominated all other samples.

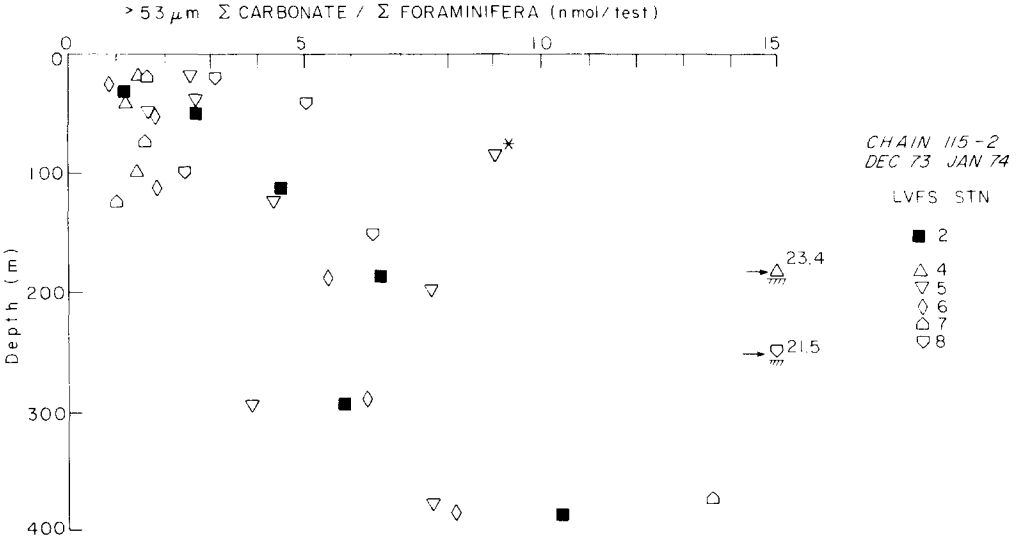

Fig. 16. >53-μm total carbonate to total Foraminifera ratio indicating the enrichment of the large particles with coccoliths. (*) indicates the 70% contribution of 350- to 520-μm *Orbulina universa* to the >53-μm carbonate at LVFS Sta. 5.

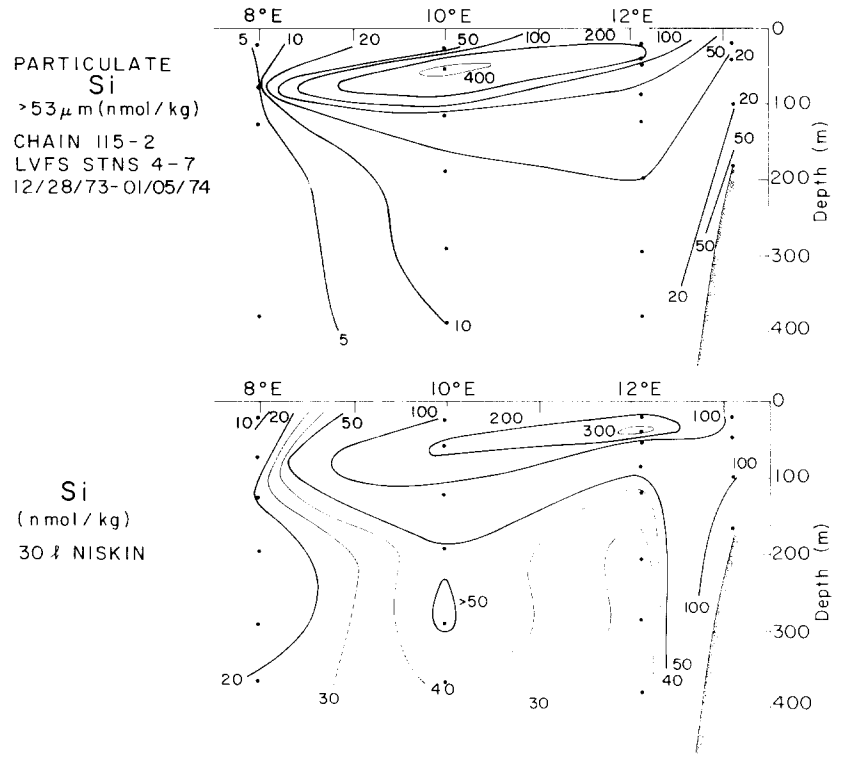

Fig. 17. Particulate silicate for > 53-μm and Niskin-0.4-μm Nuclepore fractions at LVFS Stas. 4 to 7. The Niskin method did not show the maximum at 52 m at Sta. 6.

Coccolithophorids are an important source of particulate carbonate. They determine the < 53-μm distributions of all samples and those of the > 53-μm fraction below 100 m.

Silicate

The > 53-μm silicate distribution resembles that of diatoms (Figs. 17 and 5). At Sta. 6, the Si and solenoid diatom maxima are coincident. Centrate diatoms determine the other near-surface features of the Si distributions. The highest Si concentration is at Sta. 8 where the opal content per centrate diatom frustule can be estimated to be 0.24 nmol, twice that found at Sta. 2.

The < 53-μm Si distribution could not be determined directly and so must be estimated from the analysis of Nuclepore filters from filtered 30-l. Niskin samples (Si_{nis}, Table 3). Station 4 data show opal percentages increasing with depth from 1 to 30%, consistent with diatoms being minor contributors to the biomass. The near-bottom Si maximum indicates either that productivity is usually siliceous or that opal-rich particles are transported by surface currents onto the shelf from offshore areas of higher opal productivity. Opal percentages averaged 16, 25, and 6% at Stas. 5, 6, and 7, reflecting the near-surface maxima; values were 40% at Sta. 8. The horizontal gradients of Niskin-Si and < 53-μm carbonate distributions are different, indicating that fine particles may have short residence times within the upper 400 m, their distributions being controlled by the local population of grazing organisms.

Table 3. Particulate silicate concentrations from 0.4-μm Nuclepore filters.

STATION	Z (m)	P.M. (μg kg^{-1})	Si (nmol kg^{-1})	Opal (wt%)
CH 115-2-4				
21°28'S,13°07'E	19	598.	81.9	0.9
12/28/73	48	47.5	92.2	13.6
	97	41.4	96.0	16.2
	165	76.6	342.	31.3
CH 115-2-5				
22°36'S,12°07'E	20	84.3	203.3	16.9
12/30-31/73	40	162.3	311.2	13.4
	57	37.9	90.7	16.8
	86	29.4	55.9	13.3
	119	16.1	35.5	15.4
	209	10.4	24.4	23.2
	285	14.8	27.9	17.9
	380	11.3	21.3	13.2
CH 115-2-6				
25°10'S,10.01°E	24	39.1	102.7	18.4
1/03/74	58	60.9	223.9	25.7
	122	21.0	73.2	24.4
	193	17.4	49.0	19.7
	289	14.0	52.3	26.2
	366	9.4	42.8	31.9
CH 115-2-7				
25°22'S, 7°58'E	19	45.6	8.5	1.3
1/05/74	72	66.0	16.3	1.7
	125	24.6	21.9	6.2
	182	-	11.7	(6.)
	288	73.0 (?)	13.5	(6.)
	365	7.6	23.3	21.5
CH 115-2-8				
33°18'S,17°36'E	19	693.	1992.	20.2
1/09/74	47	410.	2682.	45.8
	94	84.9	639.	52.7
	141	137.6	855.	43.5
	198	210.	1281.	42.7

Opal wt % calculation assumes 70 g mol^{-1} Si.

The <53-μm Si concentrations can be estimated in several ways:

$$<53\text{-}\mu\text{m Si} = \text{Si}_{\text{nis}} - >53\text{-}\mu\text{m Si} \tag{1}$$

$$<53\text{-}\mu\text{m Si} = \text{Si}_{\text{nis}} \tag{2}$$

$$<53\text{-}\mu\text{m Si} = \left(\frac{<53\text{-}\mu\text{m dry wt} - <53\text{-}\mu\text{m chem wt}}{0.07}\right) \tag{3}$$

$$<53\text{-}\mu\text{m Si} = \frac{(\text{Si}_{\text{nis}})}{(\text{Wt}_{\text{nis}})} \times (<53\text{-}\mu\text{m dry wt}). \tag{4}$$

Equation (1) gives negative results, particularly in near-surface samples, due to the sampling bias of the Niskin filtration method and is not preferred. Equation (2) is based on the conclusions of BISHOP and EDMOND (1976). Equation (3) uses the assumption that the difference between <53-μm dry weight and summed chemical analyses (chem wt, Table 1) is equivalent to the weight of opal; this is limited to samples from regions where aluminosilicate particles are rare relative to opal. The conversion factor between μg opal and nmol Si is 0.07. Equation (4) is based on the assumption that the weight fractions of opal in the Niskin and <53-μm fractions are equal. All four equations can be applied to samples below 100 m, but equations (2) to (4) appear to be closest to reality.

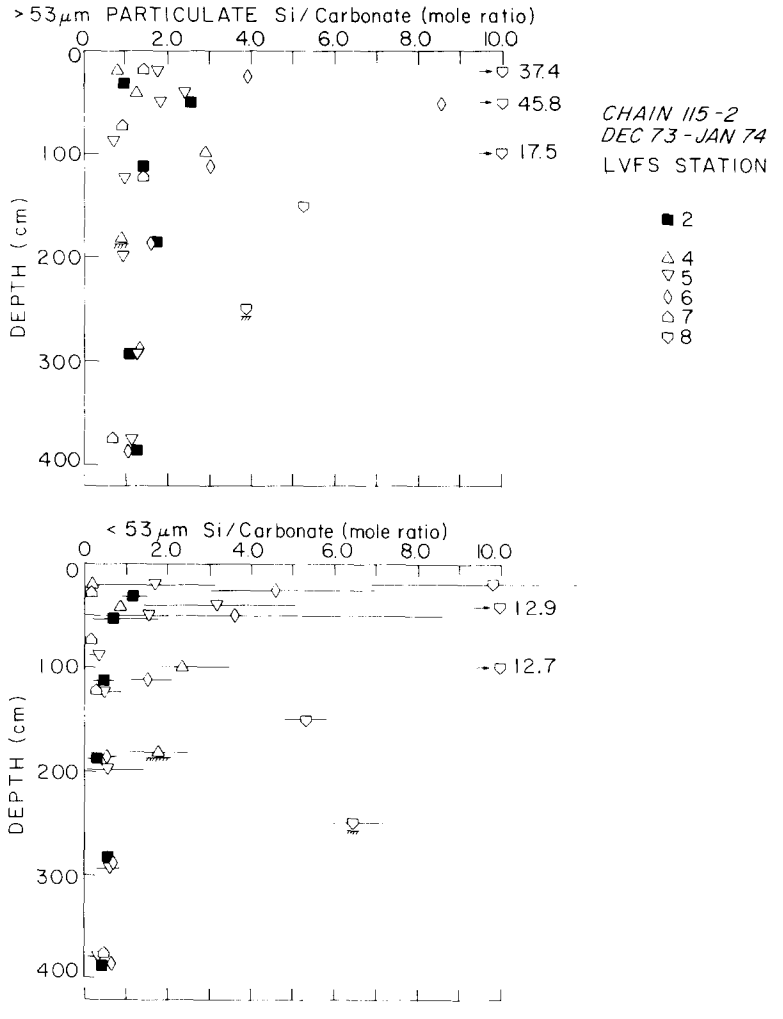

Fig. 18. >53- and <53-μm particulate $Si/CaCO_3$ ratios at LVFS Stas. 2 and 4 to 8. The intense diatom productivity at Sta. 8 is reflected in the observed ratios. Error bars in the lower figure represent the range of values calculated using the different means of estimating the <53-μm Si concentrations: lower limit based on the assumption that the Niskin method sampled the total particulate mass (samples below 100 m only).

Silicate and carbonate

The distributions of dissolved Si and specific alkalinity co-vary over much of the world's oceans, indicating that opal and carbonate are regenerated in a ratio of 2 to 1; departure from this relationship is observed in the North Pacific and Antarctic (EDMOND, 1974) where siliceous organisms dominate (LISITZIN, 1972). The Si/carbonate values of the >53-μm particles should reflect this variability.

The >53-μm samples shallower than 60 m had Si/carbonate values ranging from 0.8 (Sta. 4) to 46.0 (Sta. 8). Ratios decreased regularly with depth and the 400-m values (close to the computed values for the particle flux) are 1.15, 1.05, and 0.70 at Stas. 5, 6, and 7, compared

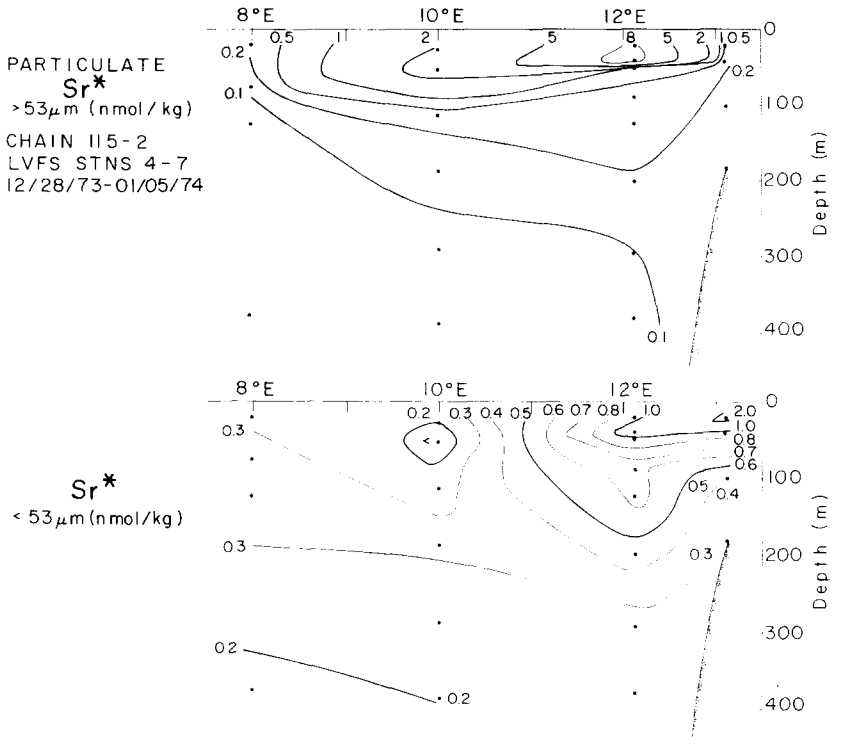

Fig. 19. >53- and <53-μm particulate non-carbonate Sr (Sr*). The >53-μm data reflect the distributions of Acantharia in the surface waters.

with 1.25 at Sta. 2. The decrease with depth can be explained by grazing organisms, reworking the large particles incorporating Si-poor material as they sink through the upper 400 m. Preferential dissolution of Si relative to carbonate may also occur (NELSON and GOERING, 1977).

Strontium

Most particulate Sr is produced by Acantharia in the surface layer. These organisms are found exclusively in the >53-μm fraction and are of interest because they are potential carriers of ^{90}Sr and perhaps trace elements into the deep ocean. Besides being present as $SrSO_4$, Sr is a minor component of carbonate and is also present at ion-exchangeable sites on organic matter. Sr*, non-carbonate Sr, is calculated according to BISHOP *et al.* (1977):

$$Sr^* = Sr - 0.0017 \times \text{carbonate}. \quad (5)$$

The >53-μm Sr* (Fig. 19) shows near-surface maxima at all stations, with an intense maximum at Sta. 5. This reflects the population of Acantharia. Vertical concentration gradients are most pronounced for Sr* indicating predation on the Acantharia and dissolution of $SrSO_4$ with depth (BISHOP *et al.*, 1977).

The >53-μm Sr*/Sr ratios decrease from surface values near unity to 0.8 near 400 m at Stas. 5, 6, and 7, comparable with the trend at Sta. 2. Near-bottom samples at Stas. 4 and 8 have lowest ratios.

The < 53-μm Sr* has near-surface maxima at Stas. 4 and 8 and deeper maxima at the other stations. The < 53-μm carbonate maximum at 88 and 124 m at Sta. 5 is a weak feature in the Sr* data. The Sr*/Sr ratios decrease from 0.8 near surface to 0.65 to 0.50 at 400 m at Stas. 5, 6, and 7; near-bottom samples from Stas. 4 and 8 have values near 0.5.

The trend to the Sr* data suggests that Sr* is more rapidly supplied to the deeper waters at stations of high productivity. Concentration levels relative to other inorganic components are lowest in cases where the rate of supply was low (Sta. 7) or the particles were exposed to seawater longer (near-bottom samples at Stas. 4 and 8).

VERTICAL FLUX OF LARGE PARTICLES THROUGH 400 M

BISHOP *et al.* (1977) demonstrated that most of the vertical flux of particulate material at Sta. 2 was carried by fecal matter. Fecal pellets and Foraminifera were minor contributors to the sediments of this area. It is important to know whether sinking fecal material is generally the dominant means by which small particles, such as coccoliths, enter the deep ocean. Fine particles may contribute substantially to the vertical flux in areas of low productivity.

Approximately 1/20th of each > 53-μm sample from 400 m at Stas. 5, 6, and 7 was scanned at 100× to determine the size distributions of fecal pellets, fecal matter, and Foraminifera. The fecal matter size distributions were extended by placing the whole samples on a light table and counting the particles larger than 1 mm.

The particle distributions (Figs. 20, 21, and 22) are plotted as frequency histograms (Foraminifera and fecal pellets) and also as log cumulative number greater than size, d, versus log d following MCCAVE (1975).

The use of cumulative distributions was introduced by JUNGE (1963), who found that the size distribution of atmospheric aerosols followed:

$$\frac{dn}{d(\log r)} = cr^{-\beta}, \tag{6}$$

where n is the number of particles smaller than radius, r, and β and c are constants. MCCAVE (1975) reviewed the application of this distribution law to Coulter Counter measurements and showed that oceanic particulate matter from below 200 to 400 m had cumulative number–size distributions which followed:

$$N = ad^{-m}, \tag{7}$$

where N is the number of particles larger than diameter, d (μm); m is the slope and a is the d = 1 μm intercept of the log N versus log d plot. This equation can be derived from equation (6). MCCAVE (1975) found that particles in the size range 1 to 100 μm were described by Junge distributions having m values between 2.4 and 3.6 and a values between 10^3 and 10^4.

The m and a values have been determined for the distributions of Foraminifera, foraminifera fragments, fecal pellets, and fecal matter (Table 4). The slopes of the Junge distributions average 5.7 (range 4.6 to 7.7) for Foraminifera; 5.3 (range 4.1 to 6.3) for foraminifera fragments; 3.8 (range 2.8 to 4.6) for fecal pellets; and 4.3 (range 3.8 to 4.9) for fecal matter. Both the m and a values are higher than those found by MCCAVE (1975), indicating that the large and small particles have different distributions. Because m values exceed 3, the volume of material in logarithmic size intervals decreases with increasing size. This is contrary to the conclusions of SHELDON, PRAKASH and SUTCLIFFE (1972).

The trend to higher m values with increasing particle size indicates that the distributions can be extrapolated using equation (7) to give maximum concentration estimates of particles

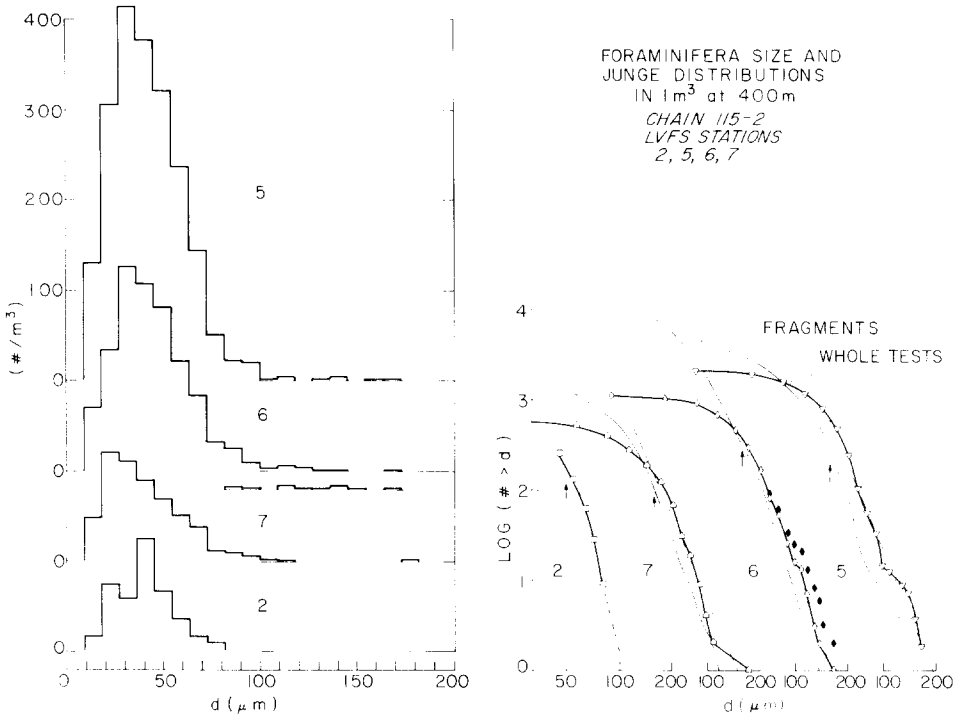

Fig. 20. Foraminifera size and Junge distributions in 1-m^3 samples from 400 m at LVFS Stas. 2, 5, 6, and 7. Subsamples of 53-μm filter, equivalent to 0.56, 0.95, and 0.96 m^3 of seawater, were scanned at 100 × to generate the distributions at Stas. 5, 6, and 7. The size distribution of pteropod shells (?) is indicated separately at Sta. 6; they are included in the Foraminifera Junge distributions (solid symbols).

present only in volumes of seawater exceeding 1 m^3. Such an extrapolation depends on particles being uniform in nature and origin but may be incorrect, either if the sample includes no particles of a given type or if no distinction is made between particle types. For instance, the extrapolation of the Junge distribution for Foraminifera at Sta. 5 predicts a concentration of 0.1 m^{-3} larger than 310 μm in diameter and 0.01 m^{-3} larger than 500 μm. A survey of the sample indicated a concentration of 0.5 m^{-3} of 430- to 480-μm *Orbulina universa*, approximately 50 times that predicted. The *O. universa* tests had a distinct distribution relative to the globigerinoid Foraminifera at this station. Accepting this note of caution, the Junge distributions will be used later to extrapolate the fecal pellet and Foraminifera fluxes.

Foraminifera concentrations at 400 m were 2090, 1110, and 560 m^{-3} at Stas. 5, 6, and 7, reflecting the population distributions in surface waters (Figs. 20 and 4). The 400-m sample at Sta. 6 also had 10 m^{-3} of 100- to 200-μm pteropod tests (tentatively identified), as well as the most abundant foraminifera and pteropod fragments. An interesting feature of all stations is the close correspondence of *m* values for Foraminifera and foraminifera fragments indicating that a common process; e.g. predation, may control their distributions.

Fecal pellet concentrations were 164, 143, and 44 m^{-3} at Stas. 5, 6, and 7, compared to 110 m^{-3} at Sta. 2 (Fig. 21). Fecal matter concentrations were most dynamic in range of size

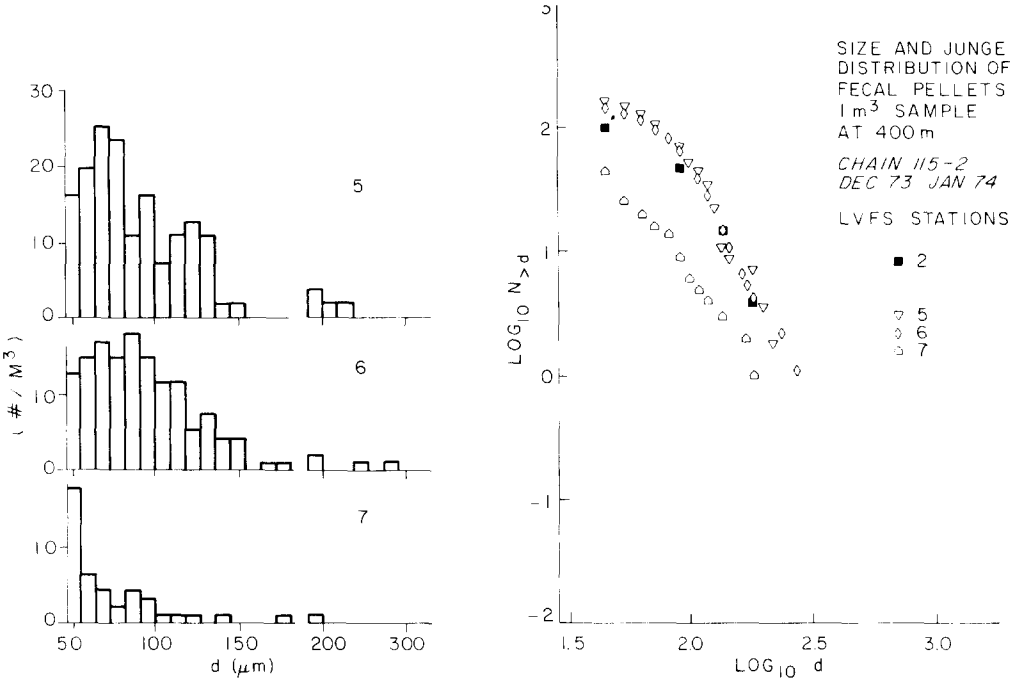

Fig. 21. Size and Junge distributions for fecal pellets in the >53-μm fraction samples from 400 m at LVFS Stas. 2, 5, 6, and 7.

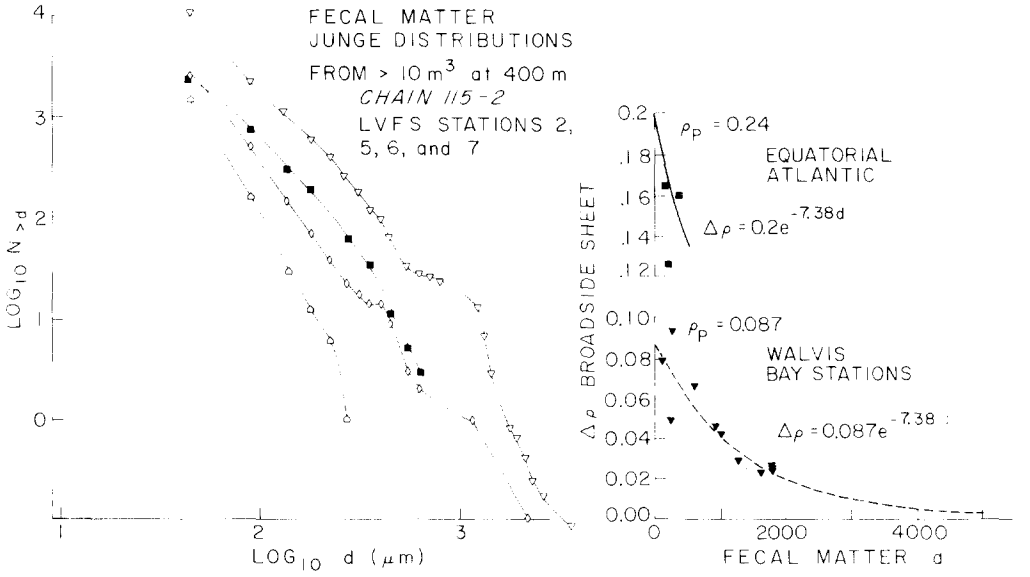

Fig. 22. Junge distributions of fecal matter at LVFS Stas. 2, 5, 6, and 7; density parameters for fecal matter from LVFS Stas. 2 and 5.

Table 4. Junge distribution parameters of > 53 μm particles at LVFS Stas. 2, 5, 6 and 7.

Station	Diameter† interval (μm)	# points fit	a	m
Foraminifera	[ρ_p = 0.5 g cm^{-3}, $\Delta\rho$†† = 0.3 g cm^{-3}]			
5	55-173	11	1.0×10^5	4.8
6	64-173	10	2.5×10^6	5.6
6*	82-173	8	2.0×10^5	4.9
7	55-183	8	8.8×10^3	4.6
2	64- 91	3	5.7×10^9	7.7
Foraminifera fragments				
5	64-146	4	1.2×10^3	4.1
6	64-146	8	3.3×10^7	6.3
7	62-128	6	1.7×10^5	5.4
Fecal pellets	[ρ_p = 0.5 g cm^{-3}, $\Delta\rho$†† = 0.2 g cm^{-3}]			
5	119-237	7	6.9×10^3	4.1
6	128-292	8	1.3×10^3	3.7
7	82-201	8	2.7×10^0	2.8
2	137-228	2	9.8×10^4	4.6
Fecal matter	[ρ_p = 0.087 g cm^{-3}, $\Delta\rho$†† = 0.087 g cm^{-3}]			
5	913-3652	9	8.2×10^9	4.9
6	913-2374	5	1.5×10^7	4.3
7	91- 320	5	3.2×10^4	4.2
	[ρ_p = 0.24 g cm^{-3}, $\Delta\rho$†† = 0.2 g cm^{-3}]			
2	234-730	5	1.0×10^5	3.8

*Includes pteropod shells (?).

†The Junge distribution parameters *a* and *m* were determined by linear least squares fit over the size interval indicated.

††Assumed density parameters used in flux models.

and concentration, being most abundant at Sta. 5 (Fig. 22). The largest particles at Stas. 5 and 7 were 4000 and 350 μm in diameter, respectively.

The morphology of fecal matter is varied. Larger particles (Fig. 23) may contain sizable Foraminifera, Acantharia, Radiolaria, crustacean carapace fragments and appendages, and fecal pellets in addition to coccoliths, coccospheres, whole and fragmented diatom frustules, and a variety of unidentifiable small particles. Virtually every kind of particle observed individually on the 53-μm mesh can be found within fecal matter.

Vertical flux models

Two models will be used to estimate mass fluxes of Foraminifera, fecal pellets, and fecal matter. Such calculations depend on our knowledge of settling behavior of each kind of particle. In the case of fecal pellets and Foraminifera this is fairly well known; however, the sinking behavior of fecal matter had not been investigated because no method of sampling had either trapped these particles or preserved their morphology. The calculations below are, in the worst case, good to an order of magnitude; their value lies in the systematic comparison of flux between stations. Flux estimates are also representative of the time of sampling; temporal variations can be expected.

Model 1: Foraminifera and fecal pellets. BISHOP *et al.* (1977) developed a vertical flux model for Foraminifera and fecal pellets based on Stokes' Law:

$$\Phi_{d_1} = \frac{n_d g \pi \Delta\rho \rho_p d^5}{108\eta} \text{g cm}^{-2}\,\text{s}^{-1} \tag{8}$$

or,

$$\Phi_{d_1} = 6 \times 10^{13} n_d \Delta\rho' \rho_p d^5 \text{ g cm}^{-2}\,1000\,\text{yr}^{-1}, \tag{9}$$

where Φ_{d_1} is the vertical flux of n_d particles of size d per ml of dry weight density, ρ_p, and density contrast (with seawater), $\Delta\rho$, sinking through seawater of viscosity η, g is the gravitational acceleration, $\Delta\rho'$ (obtained from the literature) is the effective density contrast of the particle with seawater if it fell according to Stokes' Law. η varies by less than 4% at the 400-m sample depth at all stations and is assumed to be constant at 0.0144 poise. The density parameters, $\Delta\rho'$ and ρ_p, are included in Table 4. The total mass flux from the *measured* size distributions is:

$$\Phi_{\text{meas}\cdot 1} = \sum_d \Phi_{d_1} \text{ g cm}^{-2}\,1000\,\text{yr}^{-1}. \tag{10}$$

Model 2: fecal matter. The settling behavior of fecal matter is poorly determined (BISHOP *et al.*, 1977). Its important contribution to the vertical flux at Sta. 2 necessitated laboratory sinking experiments. Dry weight densities of individual fecal matter particles, removed from the Sta. 2 and 5- to 400-m samples, were calculated using microscopic measurements of cross-sectional area and thickness and particle weight. The particles were degassed under vacuum in small beakers filled with distilled water before being transferred to the settling column (1-l. graduated cylinder filled with 28°C distilled water) using a wide mouth transfer pipette. The particle, trapped on the meniscus at the pipette tip, was immediately released upon immersion of the pipette and its travel times recorded as it passed the 100-ml graduations of the cylinder. Values were rejected if the particle came within 1 cm of the cylinder wall.

The fecal matter was approximately disk shaped and sank broadside to the direction of travel. Therefore, the equation for the sinking velocity of a broadside disk (LERMAN, LAL and DACEY, 1975) was used for comparison with the measured fall velocities:

$$v_d = \frac{g\Delta\rho h d}{10.2\eta} \text{cm s}^{-1}, \tag{11}$$

where the disk thickness, h, was determined empirically as

$$h = 0.052d + 0.0045 \text{ cm}, \tag{12}$$

and d is the disk diameter with equivalent surface area. $\Delta\rho$ was calculated using the measured fall velocities (Fig. 22). This parameter decreases exponentially with d:

$$\Delta\rho = f\Delta\rho^\circ \text{ g cm}^{-3}, \tag{13}$$

where $\Delta\rho^\circ$ is the density contrast of the particles of smallest diameter and

$$f = e^{-7.38d}. \tag{14}$$

The empirically determined equation for fecal matter settling velocity is:

$$v_{d_2} = \frac{g\Delta\rho^\circ f h d}{10.2\eta} \text{cm s}^{-1}. \tag{15}$$

The mass concentration of particles of size d is given by:

$$m_{d_2} = \frac{n_d \rho_p \pi d^2 h}{4} \text{ g cm}^{-3}. \tag{16}$$

The values for ρ_p were determined to be 0.24 and 0.087 g cm^{-3} for fecal matter at Stas. 2 and 5.

The vertical flux of fecal matter is therefore:

$$\Phi_{d_2} = v_{d_2} m_{d_2} \text{ g cm}^{-2} \text{ s}^{-1} \tag{17}$$

$$\Phi_{d_2} = 1.67 \times 10^{14} n_d \rho_p \Delta\rho^2 f h^2 d^3 \text{ g cm}^{-2} \text{ 1000 yr}^{-1}, \tag{18}$$

and the total flux for *measured* size distributions is:

$$\Phi_{\text{meas.}_2} = \sum_d \Phi_{d_2} \text{ g cm}^{-2} \text{ 1000 yr}^{-1}. \tag{19}$$

Extrapolation of the vertical flux using the Junge distributions is accomplished by calculating n_d:

$$n_d = a[(d - \Delta d/2)^{-m} - (d + \Delta d/2)^{-m}] \text{ ml}^{-1}, \tag{20}$$

where Δd is the size interval used in the size distributions of Foraminifera and fecal pellets (10^{-3} cm) and of fecal matter (5×10^{-3} cm). The extrapolation limit is determined by maximum typical size of Foraminifera in sediments (500 μm, BERGER and PIPER, 1972) and of fecal pellets (500 μm, WIEBE, BOYD and WINGET, 1976) collected by sediment trap. The size limit for fecal matter is unknown but very large.

The extrapolated mass flux, Φ_{Junge}, is added to that calculated up to a size limit of D μm from the measured size distributions:

$$\Phi_{\text{total}} = \Phi_{\text{meas}}{}_{d=1 \to D} + \Phi_{\text{Junge}}{}_{d=D \to \text{limit}} \text{ g cm}^{-2} \text{ 1000 yr}^{-1}. \tag{21}$$

D equals 100 μm for fecal pellets and Foraminifera and is nearest the largest size measured for fecal matter.

Vertical fluxes through 400 m

Measured and extrapolated size distributions of Foraminifera, fecal pellets and fecal matter are used to calculate vertical mass fluxes (Fig. 24 and Table 5). The Foraminifera flux was greatest at Sta. 5 where *Orbulina universa* contributed approximately 75% of the total:

Table 5. Calculated particle flux through 400 m (g cm^{-2} 1000 yr^{-1}).

STATION	FORAMINIFERA		FECAL PELLETS		FECAL MATTER		TOTAL		INTEGRATED† >53 μm P.M. per cm^{-2}
	meas.	total	meas.	total	meas.	total	meas.	total	
5	0.159	0.277	0.266	0.529	3.939	4.032	4.364	4.838	3.77
5**	1.173	1.291					5.378	5.852	
6	0.099	0.134	0.334	0.576	0.401	0.477	0.834	1.187	0.63
6*	0.139	0.248					0.874	1.301	
7	0.043	0.085	0.037	0.181	0.025	0.029	0.105	0.295	0.10
2	0.022	0.029	0.091	0.372	1.847	2.783	1.960	3.184	0.22

* Includes pteropod (?) flux.

** Includes flux contributed by *Orbulina universa*.

† Integrated >53-μm P.M. over upper 400 m is assumed proportional to productivity.

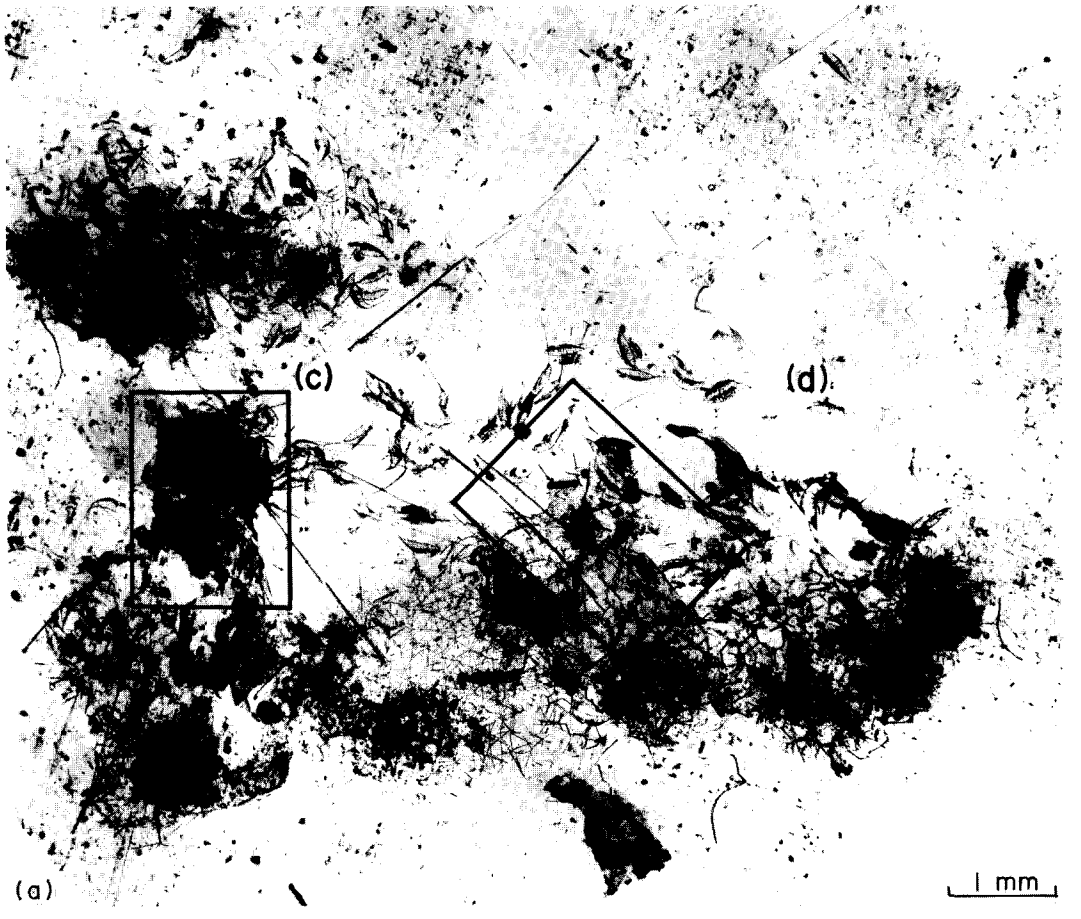

Fig. 23. (a) Composite of micrographs of a single fecal matter particle from 379 m, Sta. 5. The particle is 9 mm in length with an average diameter of 4 mm. Organisms include Acantharia, Foraminifera, Radiolaria, and intact copepods. (b) Polarized light micrograph of particle *a* demonstrating birefringent material; the structures are primarily calcium carbonate and chitin. (c) Polarized light micrograph of globigerinoid foraminifera in the particle. (d) Enlargement of a section of *a* with copepods, Acanthochiasmid acantharia, and several species of Radiolaria.

[*facing p.* 1154]

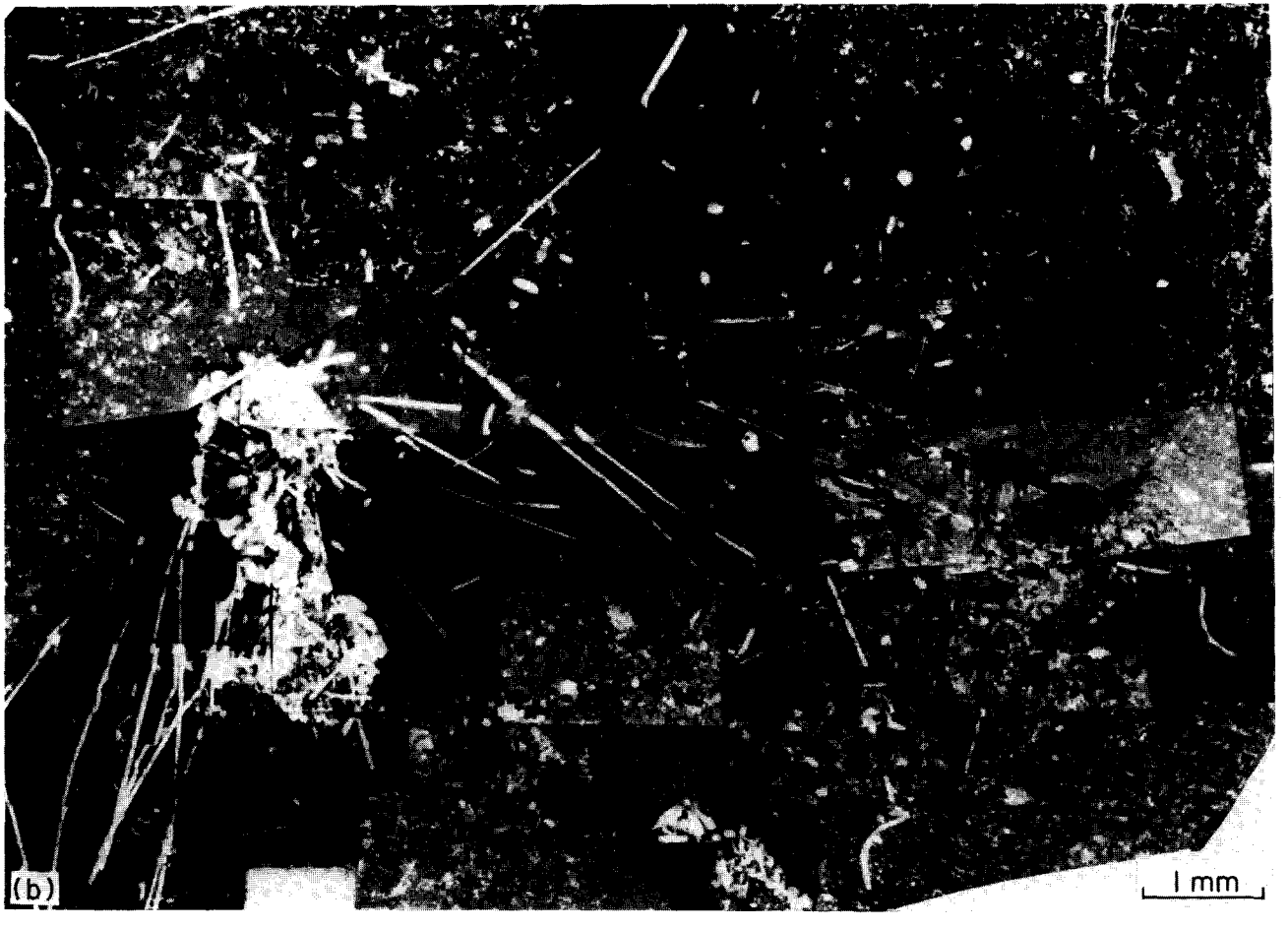

Fig. 23(b).

Fig. 23(c).

Fig. 23(d).

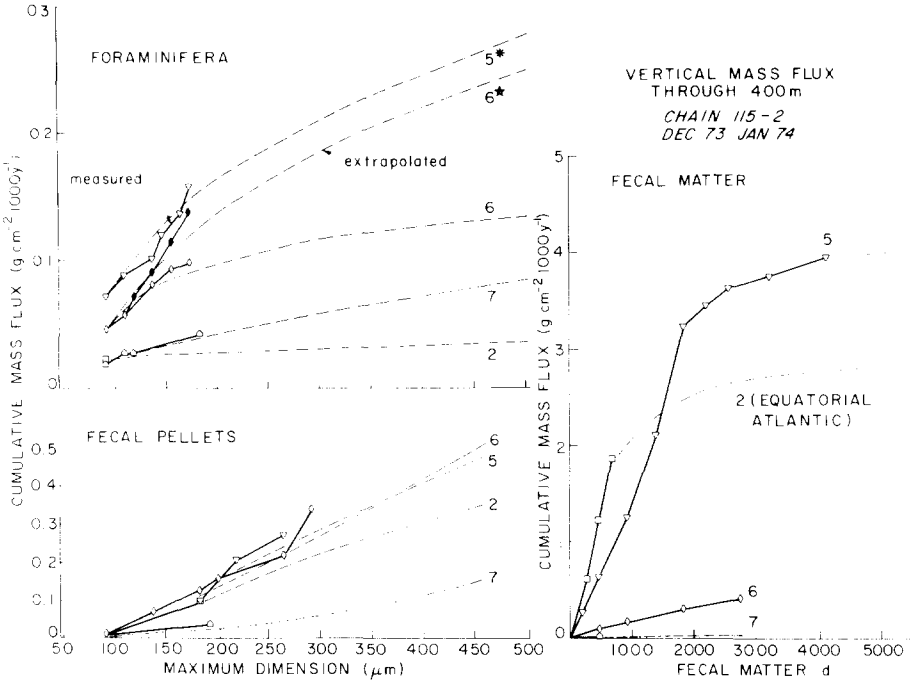

Fig. 24. Cumulative mass fluxes through 400 m at LVFS Stas. 2, 5, 6, and 7 for Foraminifera, fecal pellets, and fecal matter. ∗: Foraminifera flux = 1.3 g cm^{-2} 1000 yr^{-1} including *Orbulina universa* at Sta. 5. ★: solid symbols indicate carbonate flux including pteropod (?) tests at Sta. 6.

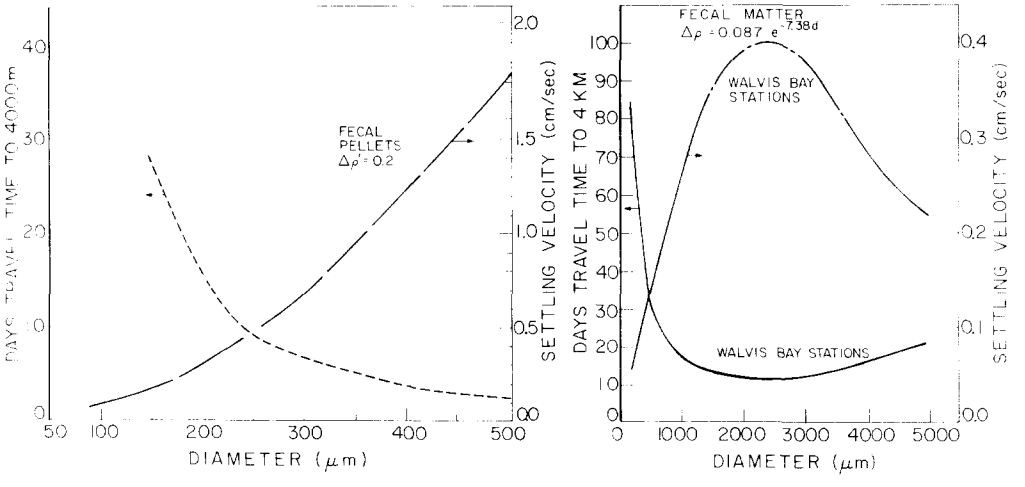

Fig. 25. Model settling behavior as a function of size for fecal pellets and fecal matter. The diagrams illustrate the differences between a Stokes' Law model (left) and that derived for fecal matter.

Table 6. Major component analysis of > 53 μm *fecal material from* 400 m *at Stas.* 2, 5, 6, *and* 7 (nmol kg^{-1}).

Station	∑ $CaCO_3$	Forams	Net F.M.	∑ Si	Rads	Diatoms	Net F.M.	$Si/CaCO_3$ F.M.
5	11.86	0.71	11.15	13.53	1.84	0.44	11.25	1.01
6	9.51	0.50	9.01	9.97	0.72	0.12	9.13	1.01
7	3.85	0.18	3.67	2.53	0.37	0.07	2.09	0.57
2	3.0	0.15	2.85	4.1	0.63	0.24	3.23	1.13

FECAL MATERIAL	WEIGHT % C_{org}	WEIGHT % $CaCO_3$	WEIGHT % OPAL
5	24.0	23.4	16.6
6	24.0	23.4	16.6
7	24.0	28.6	11.4
2	24.0	22.5	17.5

The chemical composition of fecal pellets and fecal matter is assumed similar.

the flux was lowest at Sta. 2. About 50% of the 'Foraminifera' flux at Sta. 6 may be due to pteropods (?). A scan of the whole sample (equivalent to 20 m^3 of seawater) failed to reveal any pteropod or Foraminifera shells larger than 300 and 350 μm, consistent with their Junge distributions.

Fecal pellets relative to fecal matter make least and most contribution to the flux of fecal material at Stas. 5 and 7. Comparison of the cumulative flux and settling velocities as functions of size indicates that most material contributing to the flux sinks faster than 0.1 cm s^{-1} or would settle to 4000 m in less than 30 days (Fig. 25).

An estimate of the elemental ratios of the vertical flux was made following the procedure of BISHOP *et al.* (1977). The material on the prefilters at 400 m was assumed to be ~60% by weight organic (from Fig. 11) and therefore 24% elemental carbon. The analyses of carbonate and opal were corrected by subtracting the contributions of Foraminifera, Radiolaria, and diatoms to give the proportions of these elements in fecal material (Table 6). Applying these percentages to the total mass fluxes of fecal material gives an estimate of the chemical fluxes.

The total chemical fluxes (Table 7) for organic carbon, carbonate and opal were highest and lowest at Stas. 5 and 7, varying by over an order of magnitude. The $C_{org}/CaCO_3$ and $Si/CaCO_3$ mole ratios of particle flux decreased from values >4 and ~1 at Sta. 5 to values <3 and ~0.2 at Sta. 7. Highest ratios were at Sta. 2. The Si/carbonate ratios at the LVFS

Table 7. Calculated total chemical flux > 53-μm *particles* (mmol cm^{-2} 1000 yr^{-1}).

Station	∑ $CaCO_3$		∑ Si		∑ C_{org}		$Si/CaCO_3$		$C_{org}/CaCO_3$	
	meas.	total	meas.	total	meas.	total	meas.	total	meas.	total
5	11.43	13.44	9.97	10.87	84.10	91.22	0.87	0.81	7.36	6.79
5*	21.59	23.59					0.46	0.46	3.90	3.87
6	2.71	3.80	1.74	2.50	14.70	21.06	0.64	0.66	5.42	5.54
6*	3.11	4.95					0.56	0.51	4.72	4.26
7	0.61	1.45	0.10	0.34	1.24	4.20	0.16	0.23	2.05	2.89
2	4.58	7.39	4.85	7.89	38.76	63.10	1.06	1.07	8.46	8.53

+ includes *O. Universa* flux
★ includes pteropod (?) flux

stations are all lower than the inferred 2 : 1 dissolution flux of these components in tropical oceans (EDMOND, 1974).

If the dependence of vertical particle flux upon surface productivity can be established, then it will be possible to estimate the global flux of biogenic material from maps of surface productivity. The U.N.–F.A.O. (1972) atlas shows that the annual productivity of the surface waters in the Cape Basin varies from >1500 to <300 μmol C cm^{-2} yr^{-1} from the coast of southwest Africa near Sta. 4 to the interior of the South Atlantic gyre, which includes Sta. 7. The productivity pattern encountered at Stas. 4 to 7 was different from that implied by the map. As large particles are derived from surface waters and have residence times of several days in the upper 400 m, the integrated >53-μm particle mass may be a useful measure of productivity.

Mass fluxes for fecal matter and Foraminifera at Stas. 5 to 7 show an exponential decrease with 'productivity', while the fecal pellet flux shows a gentle decrease. The particles contributing most to the vertical flux through 400 m in areas of high and low productivity are fecal matter and fecal pellets, respectively.

The organic carbon flux also shows exponential decrease with the integrated >53-μm mass for the same stations. If the integrated >53-μm mass is linearly related to surface productivity and the productivity at Stas. 5 and 7 was 200 and 1500 mmol C cm^{-2} 1000 yr^{-1}, then 94 and $\sim 99\%$ of the organic carbon fixed by photosynthesis is recycled in the upper thermocline at these stations. Sinking material contributed $<4\%$ to the total suspended particle concentration at 400 m at all stations (Table 8).

Table 8. Suspended mass concentration summary (μg kg^{-1}).

Particle	Stn. 5	Stn. 6	Stn. 7	Stn. 2
Foraminifera	0.071	0.044 0.050	0.018	0.015
fecal pellets	0.051	0.051	0.008	0.021
fecal matter	0.734	0.105	0.030	0.346
Radiolaria	0.160	0.059	0.031	0.070
Total	1.016	0.265	0.087	0.452
measured	6.1	3.1	1.4	1.1
% >53 μm dry weight	16.6	8.6	6.2	41.1
% total dry weight	4.0	1.9	0.5	3.2

The fecal matter flux was anomalously high relative to other carriers at Sta. 2. This material differed from that of the Walvis Bay stations in that it was opaque-brown, rather than white in reflected light and was three times more dense. Therefore, there are regional differences in the composition of fecal matter. Fecal pellets and Foraminifera exhibited subtle differences among stations.

The <53-μm particle flux can be estimated using the 3×10^{-4} cm s^{-1} sinking velocity derived for this size fraction at Sta. 2 using ^{7}Be. The <0.19, <0.12, and <0.14 g cm^{-2} 1000 yr^{-1} fluxes at Stas. 5 to 7 were relatively minor compared with the >53-μm fluxes at Stas. 5 and 6 but were 40% of the total mass flux at Sta. 7.

SUMMARY AND CONCLUSIONS

The particulate biological, morphological, and chemical distributions have been determined within the upper 400 m at five LVFS stations in the Cape Basin. The results have been used to establish the oceanographic significance of many features of the particle distributions previously reported for Sta. 2.

(1) The particle maximum coincided with maxima in phytoplankton and microzooplankton. Its depth depends upon the stratification of the surface waters. The particle maximum was nearest the surface at stations where the mixed layer was absent or poorly developed, and was nearest the base of the mixed layer at the other stations.

(2) Organisms showed consistent distribution patterns. Acantharia and dinoflagellates were numerically most abundant nearest the surface. Centrate diatoms dominated the >53-μm diatom population at all stations except Sta. 6, where solenoid forms were most numerous; diatoms were maximal near the base of the mixed layer or near-surface when the mixed layer was poorly developed. Foraminifera distributions followed diatoms at most stations. Radiolaria and tintinnids were most abundant in the upper thermocline.

(3) The 1 to 53-μm C_{org}/N ratios at Stas. 4, 5, 6, and 8 were uniform at 7.3 ± 0.5 (σ). This contrasts with Sta. 7 where ratios increased with depth from 9.0 to 11.3, similar to trends found at Sta. 2. The agreement of the near-shore C_{org}/N ratios with the REDFIELD, KETCHUM and RICHARDS (1963) value of 7 implies that oceanic nutrient distributions may be controlled by production and consumption in areas of high productivity.

The < 1-μm C_{org}/N ratios were consistently lower than those of the 1- to 53-μm material, probably indicating marine bacteria in the smaller fraction. Comparable quantities of both C_{org} and N were found in the two fractions in the near-surface sample at Sta. 8, indicating an extremely high marine bacterial population.

(4) Excess Ca and K were distributed similarly in the >53-μm fraction and were measurable at 400 m only at stations in productive waters. Mg was distributed similarly as found at Sta. 2 and is probably bound in a refractory organic phase.

(5) The presence of cations in association with organic matter, either as components of cytoplasm or at ion-exchangeable and complexing sites, underscores the importance of this phase as a potential carrier of minor and trace elements. The data indicate that the proposed reduction of seawater alkalinity due to the oxidation of organic matter is 20% compensated by the substitution of some protons (assumed in the Redfield–Ketchum–Richards model equation) by cations.

(6) Particulate Ca and carbonate distributions are decoupled in areas of high diatom productivity. Ca/carbonate ratios were 2.5 at Sta. 8. C_{org}/excess-Ca ratios in near-surface samples ranged from 100 to 200. Cycling of excess-Ca is estimated to be 1 to 2 $\times 10^{13}$ mol yr^{-1}, about 20% of that estimated for carbonate production by LI *et al.* (1969). The removal ratio of Ca and carbonate from the surface mixed layer is 1.13 to 1.40, making this water a poor reference for the comparison of Ca and alkalinity distributions.

(7) The >53-μm carbonate and Foraminifera distributions in the upper 100 m were parallel with divergence observed in deeper samples due to fragmentation of Foraminifera and aggregation of coccoliths into large particles by detritivores. This process explains the 10-fold increase with depth of the >53-μm $CaCO_3$/Foraminifera ratio found at all stations.

(8) Coccolithophorids dominated the <53-μm carbonate distributions in the euphotic zone, contributing the most biomass at Sta. 4. There coccoliths comprised most of the particulate carbonate below 100 m. Some features of the deep carbonate distribution are probably advective.

(9) Diatoms were the major source of particulate Si at all stations. The < 53-μm Si was distributed differently from carbonate, contributing 50% to the total particulate mass at Sta. 8 and 1% to that of the 20-m sample at Sta. 4. Values reflected the diatom distributions in surface waters, being 15, 25, and 6% at Stas. 5, 6, and 7.

(10) The > 53-μm $Si/CaCO_3$ ratios decreased from surface values ranging from 0.8 to 45 to near unity at 400 m. The decrease may be the result of exchange of material between the sizable < 53-μm reservoir (having $Si/CaCO_3 \sim 0.5$ below 100 m) and the > 53-μm fraction. This process is governed primarily by detritivores.

(11) The > 53-μm non-carbonate strontium (Sr*) and Acantharia distributions were similar. Deeper Sr* concentrations were highest relative to other inorganic components in areas of high productivity, being determined by rates of supply of fresh material from the surface layer and dissolution.

(12) The size distributions of Foraminifera, foraminiferal fragments, fecal pellets, and fecal matter differed from those predicted by McCAVE (1975) using Coulter Counter measurements of 1- to 100-μm particles. These large particles were rarer than predicted from the Junge distribution extrapolations.

(13) Two flux models were used to calculate vertical mass fluxes of Foraminifera, fecal pellets, and fecal matter. The particles contributing most to the vertical flux sank faster than 0.1 cm s^{-1} and would reach 4000 m in less than 30 days. Fecal matter and Foraminifera were major contributors to the vertical flux at Sta. 5; fecal matter, fecal pellets and Foraminifera at Sta. 6; and fecal pellets and Foraminifera at Sta. 7. Mass fluxes at these stations ranged from 5.4 to 5.9; 0.9 to 1.3; and 0.1 to 0.3 g cm^{-2} 1000 yr^{-1}. The < 53- and > 53-μm fluxes may be comparable at Sta. 7; whether or not the fine material reaches the bottom depends upon rates of organic matter destruction and of carbonate and opal dissolution.

(14) C_{org} fluxes were calculated to be 84 to 91; 15 to 21; and 1 to 4 mmol C cm^{-2} 1000 yr^{-1} at Stas. 5, 6, and 7, indicating an exponential decrease relative to surface productivity (assumed to be linearly related to the integrated > 53-μm mass in the upper 400 m). Approximately 94 and 99% of the total carbon production is recycled within the upper 400 m at Stas. 5 and 7, indicating that efficiency is highest in low productivity areas. The $C_{org}/CaCO_3$ flux ratio decreased from > 3.5 to ~ 2.0 between Stas. 5 and 7.

(15) The $Si/CaCO_3$ flux ratio was 0.9 to 0.5; 0.7 to 0.5; and 0.1 to 0.2 at Stas. 5, 6, and 7. These values are lower than the average dissolution ratio of 2 determined from dissolved silicate and alkalinity distributions in tropical oceans (EDMOND, 1974). The difference demonstrates that the particle flux may be distinct in a given area of the ocean; however, advective processes effectively mask the local regeneration anomaly.

(16) The large particles responsible for the vertical flux of material contribute < 4% to the total suspended mass concentration of particulate matter at 400 m. Their flux may control the oceanic distributions of the many chemical elements involved in the bigeochemical cycle.

Acknowledgements—We are grateful to Captain PALMERI, COLIN SUMMERHAYES (Chief Scientist), and the crew and scientific party of the *R. V. Chain* for their help in deploying the LVFS. AMY NG determined O_2 and nutrients. ROBERT STALLARD helped with the operation of the LVFS. PHIL CLARNER analysed the samples for C and N. We would like to thank Drs. DEREK SPENCER, SUSUMO HONJO, and PETER BREWER for their assistance and constructive comments. We have benefitted from discussions with Dr. EDWARD BOYLE, ROBERT COLLIER and other members of the MIT geochemistry collective. This work was supported at MIT by the Office of Naval Research on contract N00014-75-C0291. J.K.B.B. was supported in part by the Doherty Foundation.

REFERENCES

BANG N. D. (1971) The Southern Benguela Current region in February, 1966: Part II. Bathythermography and air–sea interactions. *Deep-Sea Research*, **18**, 209–224.

BANG N. D. (1973) Characteristics of an intense ocean frontal system in the upwell regime west of Capetown. *Tellus*, **25**, 256–265.

BANG N. D. and W. R. H. ANDREWS (1974) Direct current measurements of a shelf-edge frontal jet in the Southern Benguela System. *Journal of Marine Research*, **32**, 405–417.

BENDER M. and C. GAGNER (1976) Dissolved copper, nickel and cadmium in the Sargasso Sea. *Journal of Marine Research*, **31**, 119–128.

BERGER W. H. (1968) Planktonic Foraminifera: shell production and preservation. Ph.D. Thesis, University of California, San Diego, 241 pp.

BERGER W. H. and J. W. PIPER (1972) Planktonic Foraminifera: differential settling, dissolution, and redeposition. *Limnology and Oceanography*, **17**, 275–287.

BISHOP J. K. B. (1977) The chemistry, biology, and vertical flux of oceanic particulate matter. Sc.D. Thesis, Massachusetts Institute of Technology–Woods Hole Oceanographic Institution, 292 pp.

BISHOP, J. K. B. and J. M. EDMOND (1976) A new large volume filtration system for the sampling of oceanic particulate matter. *Journal of Marine Research*, **34**, 181–198.

BISHOP J. K. B., J. M. EDMOND, D. R. KETTEN, M. P. BACON and W. B. SILKER (1977) The chemistry, biology, and vertical flux of particulate matter from the upper 400 m of the equatorial Atlantic Ocean. *Deep-Sea Research*, **24**, 511–548.

BOYLE E. A., F. SCLATER and J. M. EDMOND (1976) On the marine geochemistry of cadmium. *Nature*, **263**, 42–44.

BREWER P. G., D. W. SPENCER, P. E. BISCAYE, A. HANLEY, P. L. SACHS, C. L. SMITH, S. KAJDAR and J. FREDERICKS (1976) The distribution of particulate matter in the Atlantic Ocean. *Earth and Planetary Science Letters*, **32**, 393–402.

BREWER P. G., G. T. F. WONG, M. P. BACON and D. W. SPENCER (1975) An oceanic calcium problem? *Earth and Planetary Science Letters*, **26**, 81–87.

CALVERT S. E. and N. B. PRICE (1971) Upwelling and nutrient regeneration in the Benguela Current, October 1968. *Deep-Sea Research*, **18**, 503–523.

CARPENTER J. H. (1965) The Chesapeake Bay Institute technique for the Winkler dissolved oxygen method. *Limnology and Oceanography*, **10**, 141–143.

CHESTER R., H. ELDERFIELD, J. J. GRIFFIN, R. L. JOHNSON and R. C. PADGHAM (1972) Eolian dust along the eastern margins of the Atlantic Ocean. *Marine Geology*, **13**, 91–105.

DE DECKER A. H. B. (1970) An oxygen-depleted subsurface current off the west coast of South Africa. *Division of Sea Fisheries Investigational Report*, **84**, 24 pp.

EDMOND J. M. (1974) On the dissolution of carbonate and silicate in the deep ocean. *Deep-Sea Research*, **21**, 455–480.

FEELY R. A. (1975) Major-element composition of the particulate matter in the near-bottom nepheloid layer of the Gulf of Mexico. *Marine Chemistry*, **3**, 121–156.

GARDNER W. D. (1977) Incomplete extraction of rapidly settling particles from water samplers. *Limnology and Oceanography*, **22**, 764–768.

GORDON D. C., JR. (1971) Distribution of particulate organic carbon and nitrogen at an oceanic station in the central Pacific. *Deep-Sea Research*, **18**, 1127–1134.

GORDON D. C., JR. (1977) Variability of particulate organic carbon and nitrogen along the Halifax–Bermuda section. *Deep-Sea Research*, **24**, 257–270.

HART T. J. and R. I. CURRIE (1960) The Benguela Current. *Discovery Reports*, **31**, 123–298.

HOBSON L. A. (1971) Relationships between particulate organic carbon and micro-organisms in upwelling areas off southwest Africa. *Investigacion Pesquera*, **35**, 195–208.

HOBSON L. A. and D. W. MENZEL (1969) The distribution and chemical composition of organic particulate matter in the sea and sediments off the east coast of South America. *Limnology and Oceanography*, **14**, 159–163.

HONJO S. (1976) Coccoliths: production, transportation and sedimentation. *Marine Micropaleontology*, **1**, 65–79.

HUGHES M. N. (1972) *The inorganic chemistry of biological processes*, John Wiley, 304 pp.

JONES P. G. W. (1971) The southern Benguela Current region in February 1966: Part I., Chemical observations with particular reference to upwelling. *Deep-Sea Research*, **18**, 193–208.

JUNGE C. F. (1963) *Air chemistry and radioactivity*. Academic Press, 382 pp.

KOBLENTZ-MISHKE O. J., V. V. VOLKOVINSKY and J. G. KABANOVA (1970) Plankton primary production of the world ocean. In: *Scientific exploration of the South Pacific*. W. S. WOOSTER, editor, National Academy of Sciences, pp. 183–193.

KRISHNASWAMI S. and M. M. SARIN (1976) Atlantic surface particulates: composition, settling rates and dissolution in the deep sea. *Earth and Planetary Science Letters*, **32**, 430–440.

LERMAN A., D. LAL and M. F. DACEY (1975) Stokes' settling and chemical reactivity of suspended particles in natural waters. In: *Suspended solids in water*. R. J. GIBBS, editor, Plenum Press, pp. 17–47.

LI Y. H., T. TAKAHASHI and W. S. BROECKER (1969) Degree of saturation of $CaCO_3$ in the oceans. *Journal of Geophysical Research*, **74**, 5507–5525.

LISITZIN A. P. (1972) Sedimentation in the World Ocean. *Special Publications, Society of Economic Paleontologists and Mineralogists*, **17**, 218 pp.

MAYZAUD P. and J. L. MARTIN (1975) Some aspects of the biochemical and mineral composition of marine plankton. *Journal of Experimental Marine Biology and Ecology*, **17**, 297–310.

MCCAVE I. N. (1975) Vertical flux of particles in the ocean. *Deep-Sea Research*, **22**, 491–502.

MENZEL D. W. (1974) Primary productivity, dissolved and particulate organic matter, and the sites of oxidation of organic matter. In: *The sea*. E. D. GOLDBERG, editor, John Wiley, Vol. 5, pp. 659–678.

MULLIN J. B. and J. P. RILEY (1955) The colorimetric determination of silicate with special reference to sea and natural waters. *Analytica chimica acta*, **12**, 162–176.

MURPHY J. and J. P. RILEY (1962) A modified single solution method for the determination of phosphate in natural waters. *Analytica chimica acta*, **27**, 31–36.

NELSON D. M. and J. J. GOERING (1977) Near-surface silica dissolution in the upwelling region off northwest Africa. *Deep-Sea Research*, **24**, 65–74.

PETRUSHEVSKAYA M. G. (1971) Spumellarian and Nassellarian Radiolaria in the plankton and bottom sediments of the central Pacific. In: *The micropaleontology of oceans*. B. M. FUNNELL and W. R. RIEDEL, editors, Cambridge University Press, pp. 309–319.

REDFIELD A. C., B. H. KETCHUM and F. A. RICHARDS (1963) The influence of organisms on the composition of seawater. In: *The sea*. M. N. HILL, editor, John Wiley, Vol. 2, pp. 26–77.

SCLATER F., E. A. BOYLE and J. M. EDMOND (1976) On the marine geochemistry of nickel. *Earth and Planetary Science Letters*, **31**, 119–128.

SHELDON R. W. (1972) Size separation of marine seston by membrane and glass fiber filters. *Limnology and Oceanography*, **17**, 494–498.

SHELDON R. W., A. PRAKASH and W. H. SUTCLIFFE (1972) The size distribution of particles in the ocean. *Limnology and Oceanography*, **17**, 327–340.

UN–FAO (1972) *Atlas of the living resources of the seas*. Department of Fisheries, UN–FAO, Rome.

WANGERSKY P. J. (1976) Particulate organic carbon in the Atlantic and Pacific oceans. *Deep-Sea Research*, **23**, 457–466.

WIEBE P. H., S. H. BOYD and C. WINGET (1976) Particulate matter sinking to the deep-sea floor at 2000 m in the Tongue of the Ocean, Bahamas with a description of a new sedimentation trap. *Journal of Marine Research*, **34**, 341–354.